REPRINTED FROM: Adv. Chem Phys., Volume 70 (1988)

SOLVATION EFFECTS IN FOUR-WAVE MIXING AND SPONTANEOUS RAMAN AND FLUORESCENCE LINESHAPES OF POLYATOMIC MOLECULES

SHAUL MUKAMEL

Department of Chemistry, University of Rochester, Rochester, New York 14627

CONTENTS

I. Introduction
II. The Nonlinear Response Function for Four-Wave Mixing
III. A Molecular Microscopic Model for the Nonlinear Response Function
IV. The Factorization Approximation
V. Correlation Functions for Spontaneous Raman and Fluorescence Lineshapes
VI. Nonlinear Optics of Polyatomic Harmonic Molecules in Condensed Phases—"Eigenstate-Free" Spectroscopy
VII. Coherent versus Spontaneous Raman Spectroscopy
VIII. The Role of Vibrational Relaxation in Spontaneous Raman and Fluorescence Spectroscopy
IX. Intramolecular Vibrational Redistribution (IVR) in Ultracold Molecules in Supersonic Beams
X. An Eigenstate-Free Expression for the Nonlinear Response Function
XI. Concluding Remarks
References

I. INTRODUCTION

Four-wave mixing (4WM) processes[1-6] and spontaneous Raman and fluorescence (SRF) lineshapes[7-12] provide a sensitive spectroscopic probe for polyatomic molecules in condensed phases. A 4WM process involves the interaction of three laser fields with wavevectors $\mathbf{k}_1$, $\mathbf{k}_2$, and $\mathbf{k}_3$ and frequencies ω_1, ω_2, and ω_3, respectively, with a nonlinear medium. A coherently generated signal with wavevector $\mathbf{k}_s$ and frequency ω_s is then detected (Fig. 1), where

$$\mathbf{k}_s = \pm\mathbf{k}_1 \pm\mathbf{k}_2 \pm \mathbf{k}_3 \tag{1a}$$

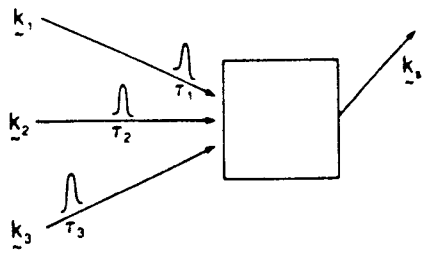

Figure 1. The general four-wave mixing process. The coherent $\mathbf{k}_s$ signal is generated by a nonlinear mixing of the three incoming fields $\mathbf{k}_1$, $\mathbf{k}_2$, and $\mathbf{k}_3$, at times τ_1, τ_2, and τ_3.

and

$$\omega_s = \pm\omega_1 \pm \omega_2 \pm \omega_3. \tag{1b}$$

Equations (1) imply that $\mathbf{k}_s$ and ω_s are given by any linear combination of the incoming wavevectors and frequencies. The various types of 4WM processes differ by the particular choices of $\mathbf{k}_s$ and ω_s [i.e., the particular choice of signs in Eqs. (1)], and by the temporal characteristics of the incoming fields. A distinction is traditionally made between frequency-domain, stationary 4WM, whereby the incoming fields and the signal field are stationary,[6,13-21] and time-domain 4WM, whereby the incoming fields are infinitely short pulses. The most common time-domain 4WM techniques are photon echoes,[22-25] transient grating,[26-33] and time-resolved coherent Raman spectroscopy.[34-43] Realistic pulsed experiments involving pulses with finite duration are characterized by a finite spectral and temporal resolution and are intermediate between these two ideal frequency-domain and time-domain limits. The SRF experiment[7-12,44-56] is illustrated in Fig. 2. It involves exciting the system with one incoming field (pulsed or steady state) and monitoring the time- and frequency-resolved emission. 4WM is a phase-matched process in which a macroscopic polarization is created, and the molecules in the sample emit in phase. This results in the directionality of the signal, as given by Eq. (1a). The SRF, on the other hand, is not phase matched, and the light is emitted in all directions.

In this chapter, we develop efficient methods for the calculation of 4WM and SRF processes of large polyatomic molecules in condensed phases (e.g., solution, solid matrices, and glasses). The key quantity in the present formulation is the nonlinear response function $R(t_3,t_2,t_1)$, which contains all the microscopic information relevant for any type of 4WM and SRF.[6,11,12,19,20,57] In Section II we introduce the nonlinear response function and derive the general formal expression for 4WM. The two ideal limiting cases of time-

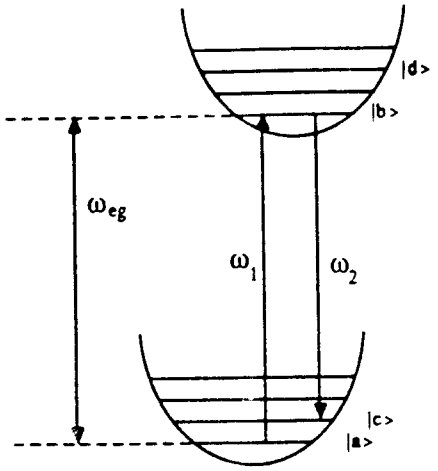

Figure 2. The level scheme for spontaneous Raman and fluorescence (SRF) spectra. $|a\rangle, |c\rangle, \ldots,$ denote vibronic states belonging to the ground-state manifold, and $|b\rangle, |d\rangle, \ldots,$ denote vibronic states belonging to the electronically excited manifold. In a SRF experiment, an ω_1 photon is absorbed, and an ω_2 photon is emitted.

domain 4WM and frequency-domain 4WM are obtained from the same unified expression. The nonlinear susceptibility $\chi^{(3)}$ that is commonly used in stationary 4WM is also expressed in terms of R. In Section III we calculate the response function for a general model system for molecular 4WM.[6,19,44,45] The model consists of two manifolds of vibronic levels coupled to a thermal bath, which causes dephasing. In general, the calculation involves a four-point correlation function of the dipole operator. This expression can also be written in Liouville space (i.e., in terms of the time evolution of the density matrix). The latter form is very useful for deriving approximate methods for evaluating the nonlinear response function. In Section IV we introduce the factorization approximation.[11,19] This approximation allows us to express any 4WM process in terms of generalized single-photon lineshape functions related to two-time correlation functions of the dipole operator. In Section V we define the time- and frequency-resolved spectrum in SRF. We show that these lineshapes may be expressed in terms of the same four-point correlation function of the dipole operator which appears in 4WM. Our final results are expressed further in terms of Liouville space propagators. Invoking again the factorization approximation results in a simple, easily calculable expression for SRF. The closed expressions derived in Sections III–V involve multiple summations (four) over molecular vibronic levels. Such summations restrict the usage of these results to relatively small molecules with a few relevant levels. In Section VI, we specialize to harmonic molecules. In this case, it is

possible to perform two out of the four summations using Green's function techniques in the time domain.[44,45,58] This results in an expression for 4WM and SRF in terms of generalized ground-state and excited-state polarizability operators. The latter are evaluated in the time-domain using Fourier transform techniques. This result is extremely useful and allows a convenient calculation of the response functions, both in the time domain and in the frequency domain. In Section VII we apply these results toward the calculation of coherent and spontaneous Raman excitation profiles in simple model systems.[45] Detailed numerical calculations provide a comparison of these lineshapes for a stochastic model of line broadening. In Section VIII we consider the effects of vibrational relaxation on SRF lineshapes and provide a simple computational scheme for incorporating these effects using the methodology of the previous sections.[59] In Section IX, we apply the model to "intramolecular solvation" and consider the SRF spectra of ultracold anthracene in a supersonic beam.[60,61] In Section X, we carry the Green's function techniques one step further and perform all the summations over vibronic states.[45] A closed expression is obtained for the nonlinear response function in the time domain, in which all the summations over molecular states have been eliminated [Eq. (57) together with Eq. (133)]. This expression is particularly useful for ideal time-domain experiments. Finally, our results are summarized in Section XI.

II. THE NONLINEAR RESPONSE FUNCTION FOR FOUR-WAVE MIXING

We consider a nonlinear optical medium, consisting of polyatomic molecules interacting with a classical external electromagnetic field by a dipolar interaction. The total Hamiltonian of the system is

$$H_T = H + H_{\text{int}}. \tag{2}$$

Here H is the Hamiltonian for the material system in the absence of the radiation field. H_{int} represents the radiation–matter interaction and is given by

$$H_{\text{int}}(t) = \sum_{\alpha} E(\mathbf{r}_\alpha, t) V_\alpha, \tag{3}$$

where V_α is the dipole operator of the molecule labeled α and located at $\mathbf{r}_\alpha$, and the summation is over all the molecules in the nonlinear medium. $E(\mathbf{r}, t)$ is the electromagnetic field, which for a general 4WM process (Fig. 1) can be decomposed into four components:

$$E(\mathbf{r},t) = \sum_{j=1}^{4} [E_j(t)\exp(i\mathbf{k}_j\cdot\mathbf{r} - i\omega_j t) + E_j^*(t)\exp(-i\mathbf{k}_j\cdot\mathbf{r} + i\omega_j t)]. \quad (4)$$

The three incoming fields $j = 1, 2, 3$ will be treated classically. For these fields, $E_j(t)$ is a classical function of time representing their temporal envelopes. The generated signal field $E_4 = E_s$ will be treated quantum mechanically, since it is generated by spontaneous emission. For that field, we have[62]

$$E_s = -i(2\pi\hbar\omega_s/\Omega)^{1/2}a_s, \quad (5a)$$

$$E_s^* = i(2\pi\hbar\omega_s/\Omega)^{1/2}a_s^\dagger. \quad (5b)$$

Here $a_s^\dagger$ (a_s) is the creation (annihilation) operator for the sth mode, and we have adopted a box normalization with Ω being the volume. In this article, we consider a simple model, in which the active nonlinear medium consists of noninteracting polyatomic molecules (absorbers) and a set of bath degrees of freedom, which do not interact with the electromagnetic field, but do interact with the absorbers. In this case, we can focus on one absorber, located at $\mathbf{r}$, and write

$$H_{\text{int}}(t) = E(\mathbf{r},t)V, \quad (6)$$

where V is the dipole operator of that absorber. The nature of the bath depends on the physical system of interest; it could be the solvent, a host crystal, an amorphous medium (glass), and so forth. For isolated large molecules the bath may consist of those vibrational degrees of freedom, which are weakly coupled to the electronic transition of interest (see Section IX). Direct interactions among the absorbers lead to interesting transport phenomena, and certain 4WM techniques, such as the transient grating,[26-33] are particularly suitable to probe these intermolecular interactions. The incorporation of transport processes in 4WM will not be considered here. In order to calculate the 4WM signal, we start at $t = -\infty$ and assume that the system is in thermal equilibrium with respect to H (without the radiation field)

$$\rho(-\infty) = \exp(-H/kT)/\text{Tr}\exp(-H/kT). \quad (7)$$

The system then evolves in time according to the Liouville equation

$$\frac{d\rho}{dt} = -i[H,\rho] - i[H_{\text{int}},\rho]. \quad (8)$$

In Eq. (8) and in the rest of this article, we set $\hbar = 1$. The formal manipulations

in this article are simplified considerably by introducing a Liouville space notation.[11,19] We define Liouville space operators L, L_{int} and $\Upsilon^{\times}$ by their action of an ordinary operator A, that is,

$$LA \equiv [H, A], \tag{9a}$$

$$L_{\text{int}}A \equiv [H_{\text{int}}, A], \tag{9b}$$

and

$$\Upsilon^{\times}A \equiv [V, A]. \tag{9c}$$

Equation (8) then assumes the form:

$$\frac{d\rho}{dt} = -iL\rho - iL_{\text{int}}\rho. \tag{10a}$$

This notation is useful, since now Eq. (10a) is formally identical to the Schrödinger equation

$$\frac{d\psi}{dt} = -iH\psi - iH_{\text{int}}\psi. \tag{10b}$$

This allows us to carry out many formal manipulations (perturbation theory, projection operator techniques, selective averaging over bath degrees of freedom, etc.) in a straightforward way. We shall be interested in calculating the polarization $\langle P(\mathbf{r}, t)\rangle$ at position $\mathbf{r}$ at time t. This is given by the expectation value of the dipole operator V:

$$\langle P(\mathbf{r}, t)\rangle \equiv \langle\langle V|\rho(t)\rangle\rangle, \tag{11}$$

where we are using the double bracket notation[11,19] to denote an inner product of operators. For any two operators,

$$\langle\langle A|B\rangle\rangle \equiv \mathrm{Tr}(A^{\dagger}B). \tag{12}$$

We shall also define a Liouville space "matrix element" by

$$\langle\langle A|L|B\rangle\rangle \equiv \mathrm{Tr}(A^{\dagger}LB). \tag{13}$$

For a 4WM process we calculate $\rho(t)$ perturbatively to third order in L_{int}. We then get[6,19]

$$\langle P(\mathbf{r},t)\rangle = (-i)^3 \int_0^\infty dt_1 \int_0^\infty dt_2 \int_0^\infty dt_3 \langle\langle V|G(t_3)L_{\text{int}}(t-t_3)G(t_2) \times L_{\text{int}}(t-t_2-t_3)G(t_1)L_{\text{int}}(t-t_1-t_2-t_3)|\rho(-\infty)\rangle\rangle. \quad (14)$$

Here the Green's function $G(\tau)$ is the formal solution of Eq. (10a) in the absence of the electromagnetic field, $L_{\text{int}} = 0$, that is,

$$G(\tau) = \exp(-iL\tau). \quad (15)$$

For subsequent manipulations, we shall also introduce the Green's function in the frequency domain

$$\hat{G}(\omega) \equiv -i\int_0^\infty d\tau \exp(i\omega\tau)G(\tau) = \frac{1}{\omega - L}. \quad (16)$$

The interpretation of Eq. (14) is as follows (Fig. 3): The system starts at $t = -\infty$ with a density matrix $\rho(-\infty)$. It then interacts three times with the electromagnetic field at times $t - t_1 - t_2 - t_3$, $t - t_2 - t_3$, and $t - t_3$. During the intervals between interactions (t_1, t_2, and t_3) it evolves in time according to $G(\tau)$. Finally, at time t we calculate the polarization. We are now in a position to introduce the formal definition of the signal in 4WM. We reiterate that the only values of $\mathbf{k}_s$ giving nonvanishing contributions to the coherent nonlinear signal are those given by Eqs. (1). Hereafter we shall make a specific choice, namely,

$$\mathbf{k}_s = \mathbf{k}_1 - \mathbf{k}_2 + \mathbf{k}_3, \quad (17a)$$

and

$$\omega_s = \omega_1 - \omega_2 + \omega_3. \quad (17b)$$

Any other combination may be obtained from our final expression [Eq. (28)]

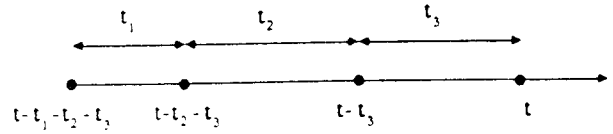

Figure 3. The time arguments in Eq. (14). The three interactions of the system with the radiation field take place at times $t - t_1 - t_2 - t_3$, $t - t_2 - t_3$, and $t - t_3$. The polarization is then calculated at time t; t_1, t_2, and t_3 are the intervals between the radiative interactions.

by changing one (or more) $\mathbf{k}_j$ and ω_j into $-\mathbf{k}_j$ and $-\omega_j$, and $E_j(t)$ into $E_j^*(t)$. We shall be interested in a parametric process, whereby the generated field ω_s satisfies the phase-matching condition [Eq. (17)], which implies that the signal is proportional to $\delta(\mathbf{k}_1 - \mathbf{k}_2 + \mathbf{k}_3 - \mathbf{k}_s)$. The generated coherent signal may be defined by considering the rate of emission of photons into the $\mathbf{k}_s$ mode. The operator representing this rate is

$$B = \frac{d}{dt} a_s^\dagger a_s = i[H_{\text{int}}(t), a_s^\dagger a_s], \tag{18a}$$

which in Liouville space notation assumes the form

$$|B\rangle\rangle = iL_{\text{int}}(t)|a_s^\dagger a_s\rangle\rangle. \tag{18b}$$

The photon emission rate at time t into mode s is the expectation value of $|B\rangle\rangle$, that is,

$$\langle\langle B|\rho(t)\rangle\rangle = \text{Tr}[B^\dagger \rho(t)], \tag{19}$$

where $\rho(t)$ is the total density matrix (system + field + bath) at time t. Since we shall consider only contributions to Eq. (19) that satisfy the phase-matching condition $\delta(\mathbf{k}_1 - \mathbf{k}_2 + \mathbf{k}_3 - \mathbf{k}_s)$, we may integrate the signal over all ω_s, without any loss of information. Our definition for the four-wave mixing signal (rate of change of the intensity of field s) will, therefore, be[45,63]

$$S(\mathbf{k}_s, t) = \int d\omega_s \langle\langle B|\rho(t)\rangle\rangle, \tag{20}$$

or, using Eq. (18b),

$$S(\mathbf{k}_s, t) = -i \int d\omega_s \langle\langle a_s^\dagger a_s | L_{\text{int}}(t)|\rho(t)\rangle\rangle. \tag{21}$$

In order to proceed further, we need to expand $\rho(t)$ to the necessary order in γ. Initially, at $t \to -\infty$, we have

$$|\rho(-\infty)\rangle\rangle = |\rho_S(-\infty)\rangle\rangle |\rho_B(-\infty)\rangle\rangle |\rho_R(-\infty)\rangle\rangle, \tag{22}$$

where ρ_S, ρ_B, and ρ_R stand for the density matrix of the system, of the bath, and of the radiation field, respectively. The system and bath are in thermal equilibrium, and mode s of the radiation field is in the vacuum state

$$|\rho_R(-\infty)\rangle\rangle = |\text{vac, vac}\rangle\rangle. \tag{23a}$$

Equation (23a) is the Liouville space notation for

$$\rho_R(-\infty) = |\text{vac}\rangle\langle\text{vac}|. \tag{23b}$$

Note, that ρ_R corresponds only to the generated mode $\mathbf{k}_s$. The incident modes $\mathbf{k}_1$, $\mathbf{k}_2$, $\mathbf{k}_3$ are treated classically and are described by the classical incident fields E_1, E_2, and E_3 [Eq. (4)]. It is clear that in order for the trace over the signal field $\mathbf{k}_s$ in Eq. (21) not to vanish, we need to apply the interaction [Eq. (3)] with mode s twice, once from the left and once from the right. If these two interactions occur with two different particles (say α and β), we obtain a factor $\exp[-i\mathbf{k}_s\cdot(\mathbf{r}_\alpha - \mathbf{r}_\beta)]$ [Eq. (4)]. If $\alpha = \beta$, that is, both interactions occur with the same particle, then we lose all information about $\mathbf{k}_s$, and the process will not be phase matched. Therefore, it is clear that we need at least two different material particles in order to achieve the phase matching [Eq. (1)]. In order to satisfy the phase-matching condition, we need to expand Eq. (21) to eighth order in V, whereby each field $\mathbf{k}_1$, $\mathbf{k}_2$, $\mathbf{k}_3$, and $\mathbf{k}_s$ interacts once with atom α and once with atom β, resulting in the spatial factor $\exp[i(\mathbf{k}_1 - \mathbf{k}_2 + \mathbf{k}_3 - \mathbf{k}_s)\cdot(\mathbf{r}_\alpha - \mathbf{r}_\beta)]$. When this factor is summed over $\mathbf{r}_\alpha$, $\mathbf{r}_\beta$, it will result in the desired phase-matching condition. The reason why we need to expand our expression [Eq. (21)] to eight order in V, is that we are looking for a four-photon process, whose amplitude is fourth order in V and intensity (amplitude square) must be eighth order in V. The density matrix $\rho(t)$ must therefore be expanded to seventh order in V in order to obtain the signal S to eighth order. We then get[63]

$$S(\mathbf{k}_s, t) = -i\int d\omega_s \langle\langle a_s^\dagger a_s | L_{\text{int}}(t) | \rho^{(7)}(t)\rangle\rangle. \tag{24}$$

After some algebraic manipulations and with the elimination of some numerical constants, the signal can be recast in the form[45,63]

$$S(\mathbf{k}_s, t) = \sum_{\alpha,\beta} \langle P(\mathbf{r}_\alpha, t) P^\dagger(\mathbf{r}_\beta, t)\rangle \exp[-i\mathbf{k}_s\cdot(\mathbf{r}_\alpha - \mathbf{r}_\beta)]. \tag{25}$$

Here $P(\mathbf{r}_\alpha, t)$, Eq. (14), is the polarization at point $\mathbf{r}_\alpha$ at time t and $P^\dagger$ is the hermitian conjugate of P. The angular brackets denote averaging over the thermal bath with which the absorbers interact. Equation (25) reflects the fact that the 4WM signal results from a coherent parametric emission, involving many particles emitting in phase. Usually, different particles in the nonlinear medium are not correlated, so that the two-body average can be factorized in the form

$$\langle P(\mathbf{r}_\alpha, t)P^\dagger(\mathbf{r}_\beta, t)\rangle = \langle P(\mathbf{r}_\alpha, t)\rangle\langle P^\dagger(\mathbf{r}_\beta, t)\rangle. \tag{26}$$

Equations (25) and (26) result in

$$S(\mathbf{k}_s, t) = |\langle P(\mathbf{k}_s, t)\rangle|^2, \tag{27a}$$

where

$$\langle P(\mathbf{k}_s, t)\rangle = \sum_\alpha \langle P(\mathbf{r}_\alpha, t)\rangle \exp(-i\mathbf{k}_s \cdot \mathbf{r}_\alpha + i\omega_s t). \tag{27b}$$

It should be noted that in the presence of long-range spatial correlations in the sample (e.g., near critical points) the factorization [Eq. (26)] does not hold, and 4WM actually probes the two-particle correlation function. This is analogous to spontaneous light scattering. A general theory of 4WM near critical points needs to be developed. A first step in this direction was made recently.[63] In the present article, we shall not consider systems with long-range spactial correlations, and we assume that Eq. (26) holds. Using Eqs. (3), (9), and (14), we then get

$$\begin{aligned}\langle P(\mathbf{k}_s, t)\rangle = (-i)^3 \sum_{m,n,q=1,2,3} \int_0^\infty dt_3 \int_0^\infty dt_2 \int_0^\infty dt_1 R(t_3, t_2, t_1) \\ \times \exp[i(\omega_m + \omega_n + \omega_q)t_3 + i(\omega_m + \omega_n)t_2 + i\omega_m t_1] \\ \times E_m(t - t_1 - t_2 - t_3)E_n(t - t_2 - t_3)E_q(t - t_3).\end{aligned} \tag{28}$$

$R(t_3, t_2, t_1)$ is the *nonlinear response function*, which contains all relevant microscopic information for any 4WM process:

$$R(t_3, t_2, t_1) = \langle\langle V | G(t_3)\mathcal{V}G(t_2)\mathcal{V}G(t_1)\mathcal{V}|\rho(-\infty)\rangle\rangle. \tag{29}$$

The summation in Eq. (28) is over all $3! = 6$ permutations of ω_m, ω_n, and ω_q with ω_1, $-\omega_2$, and ω_3, and of E_m, E_n, and E_q with E_1, E_2^*, and E_3. Alternatively, we may define the response function in the frequency domain by performing a triple Fourier transform of $R(t_3, t_2, t_1)$, that is,

$$\begin{aligned}\hat{R}(\omega_m + \omega_n + \omega_q, \omega_m + \omega_n, \omega_m) = (-i)^3 \int_0^\infty dt_3 \int_0^\infty dt_2 \int_0^\infty dt_1 \\ \times \exp[i(\omega_m + \omega_n + \omega_q)t_3 \\ + i(\omega_m + \omega_n)t_2 + i\omega_m t_1]R(t_3, t_2, t_1).\end{aligned} \tag{30}$$

Equation (28) may then be rearranged in the form

$$\langle P(\mathbf{k}_s, t)\rangle = \sum_{m,n,q=1,2,3} \int_{-\alpha}^{\alpha} d\omega'_m \int_{-\alpha}^{\alpha} d\omega'_n \int_{-\alpha}^{\alpha} d\omega'_q \times \hat{R}(\omega'_m + \omega'_n + \omega'_q, \omega'_m + \omega'_n, \omega'_m) J_m(\omega'_m) J_n(\omega'_n) J_q(\omega'_q) \times \exp[i(\omega_m + \omega_n + \omega_q - \omega'_m - \omega'_n - \omega'_q)t], \tag{31}$$

where

$$\hat{R}(\omega_m + \omega_n + \omega_q, \omega_m + \omega_n, \omega_m) = \langle\langle V | \hat{G}(\omega_m + \omega_n + \omega_q) \hat{\gamma} \hat{G}(\omega_m + \omega_n) \hat{\gamma} \hat{G}(\omega_m) \hat{\gamma} | \rho(-\infty)\rangle\rangle \tag{32}$$

and

$$J_j(\omega'_j) = (2\pi)^{-1} \int_{-\alpha}^{\alpha} d\tau\, E_j(\tau) \exp[i(\omega'_j - \omega_j)\tau], \quad j = m, n, q, \tag{33}$$

is the spectral density of the j field.

Equations (27) and (28) or alternatively Eq. (31) provide the most general formal expression for any type of 4WM process. They show that the nonlinear response function $R(t_3, t_2, t_1)$, or its Fourier transform $\hat{R}(\omega_m + \omega_n + \omega_q, \omega_m + \omega_n, \omega_m)$, contains the complete microscopic information relevant to the calculation of any 4WM signal. As indicated earlier, the various 4WM techniques differ by the choice of $\mathbf{k}_s$ and ω_s and by the temporal characteristics of the incoming fields $E_1(t)$, $E_2(t)$, and $E_3(t)$. A detailed analysis of the response function and of the nonlinear signal will be made in the following sections for specific models. At this point we shall consider the two limiting cases of ideal time-domain and frequency-domain 4WM. In an ideal time-domain 4WM, the durations of the incoming fields are infinitely short, that is,

$$\begin{aligned} E_1(\tau) &= E_1 \delta(\tau - \tau_1), \\ E_2(\tau) &= E_2 \delta(\tau - \tau_2), \\ E_3(\tau) &= E_3 \delta(\tau - \tau_3), \end{aligned} \tag{34}$$

where $\tau_1 < \tau_2 < \tau_3$ (Fig. 1). We further denote $t_1 = \tau_2 - \tau_1$, $t_2 = \tau_3 - \tau_2$, and $t_3 = t - \tau_3$. Upon the substitution of Eq. (34) into Eq. (28), we get

$$\langle P(\mathbf{k}_s, t)\rangle = E_1 E_2^* E_3 R(t_3, t_2, t_1) \exp[i\omega_1 t_1 + i(\omega_1 - \omega_2)t_2 + i(\omega_1 - \omega_2 + \omega_3)t_3] \tag{35}$$

and

$$S(\mathbf{k}_s, t) = |E_1 E_2 E_3|^2 |R(t_3, t_2, t_1)|^2. \tag{36}$$

The other extreme limit of 4WM is a stationary frequency-domain experiment in which the field amplitudes $E_1(\tau)$, $E_2(\tau)$, and $E_3(\tau)$ are time independent. In this case, we have

$$\begin{aligned} J_1(\omega_1') &= E_1 \delta(\omega_1' - \omega_1), \\ J_2(\omega_2') &= E_2 \delta(\omega_2' - \omega_2), \\ J_3(\omega_3') &= E_3 \delta(\omega_3' - \omega_3). \end{aligned} \tag{37}$$

Using Eqs. (31) and (37), we get

$$\langle P(\mathbf{k}_s, t) \rangle = \chi^{(3)}(-\omega_s, \omega_1, -\omega_2, \omega_3) E_1 E_2^* E_3, \tag{38}$$

where the nonlinear susceptibility $\chi^{(3)}$ is given by

$$\chi^{(3)}(-\omega_s, \omega_1, -\omega_2, \omega_3) = \sum_{m,n,q=1,2,3} \hat{R}(\omega_m + \omega_n + \omega_q, \omega_m + \omega_n, \omega_m). \tag{39}$$

The stationary signal [Eq. (27)] is given in this case by

$$S(\mathbf{k}_s) = |E_1 E_2 E_3|^2 |\chi^{(3)}(-\omega_s, \omega_1, -\omega_2, \omega_3)|^2. \tag{40}$$

III. A MOLECULAR MICROSCOPIC MODEL FOR THE NONLINEAR RESPONSE FUNCTION

We shall now apply the results of Section II to a specific model system, commonly used in molecular 4WM. We consider a molecular-level scheme for the absorber, consisting of a manifold of vibronic levels belonging to the ground electronic state, denoted $|a\rangle, |c\rangle, \ldots$, and a manifold of vibronic levels belonging to an excited electronic state, denoted $|b\rangle, |d\rangle, \ldots$, (Fig. 4). The ground and the electronically excited states will be denoted $|g\rangle$ and $|e\rangle$, respectively. The absorber is further coupled to a thermal bath, and the combined Hamiltonian for the molecule and the bath is[6,44,57,58,64]

$$H = |g\rangle [H_g(Q_S) + h_g(Q_B)] \langle g| + |e\rangle [H_e(Q_S) + h_e(Q_B)] \langle e|. \tag{41}$$

Here the ground-state Hamiltonian is partitioned into a system part H_g, which

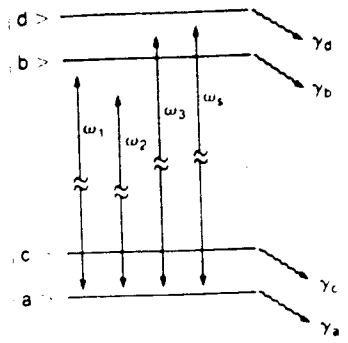

Figure 4. The molecular-level scheme and laser frequencies for 4WM. Levels $|a\rangle$ and $|c\rangle$ are part of the ground-state vibrational manifold, whereas levels $|b\rangle$ and $|d\rangle$ belong to an electronically excited manifold. γ_v is the inverse lifetime of level $|v\rangle$. The electronic dipole operator [Eq. (47)] couples vibronic states belonging to different electronic states.

depends on the system coordinates Q_S, and a bath part h_g, which depends on the bath coordinates Q_B. Similar partitioning of the excited-state Hamiltonian into H_e and h_e is made. The interaction between the system and the bath is reflected in the difference between h_g and h_e, which implies that the bath eigenstates are different, depending on the electronic state of the system. The Hamiltonian [Eq. (41)] does not couple the bath directly to the molecular vibrational degrees of freedom. The key physical assumption underlying Eq. (41) is that a polar solvent is mainly sensitive to the molecular charge distribution, which may be very different for the ground $|g\rangle$ and the electronically excited $|e\rangle$ states. The difference between h_g and h_e results in the solvent reorganization upon electronic excitation of the molecule.[65] The interaction of the solvent with the molecule is only weakly dependent on the nuclear coordinates and this dependence is ignored in Eq. (41). This interaction results in solvent-induced vibrational relaxation, which may play an important role in molecular spectra in condensed phases. In Section VIII we incorporate the vibrational relaxation in our theory, thus eliminating the major approximation of Eq. (41). The eigenstates of the ground-state and of the excited-state Hamiltonians will be denoted as (Fig. 4)

$$(H_g + h_g)|v\alpha\rangle = (\varepsilon_v + \varepsilon_\alpha)|v\alpha\rangle \qquad v = a, c, \ldots \tag{42a}$$

and

$$(H_e + h_e)|v\beta\rangle = (\varepsilon_v + \varepsilon_\beta)|v\beta\rangle \qquad v = b, d, \ldots . \tag{42b}$$

Here a, b, c, d, ... stand for the collection of all system quantum numbers,

whereas α and β represent all the bath quantum numbers. The molecule is taken to be initially at thermal equilibrium in the ground-state manifold, and its density matrix is the direct product of the system (σ_g) and the bath (ρ_g) components, that is,

$$\rho(-\infty) = \sigma_g(Q_S)\rho_g(Q_B) \tag{43}$$

with

$$\sigma_g = \exp(-H_g/kT)/\mathrm{Tr}\exp(-H_g/kT) = \sum_a |a\rangle P(a)\langle a|, \tag{43a}$$

$$\rho_g = \exp(-h_g/k\Gamma)/\mathrm{Tr}\exp(-h_g/kT) = \sum_\alpha |\alpha\rangle \rho_g(\alpha)\langle\alpha|. \tag{43b}$$

Here

$$P(a) = \exp(-\varepsilon_a/kT)\Big/\sum_a \exp(-\varepsilon_a/kT), \tag{44a}$$

$$\rho_g(\alpha) = \exp(-\varepsilon_\alpha/kT)\Big/\sum_\alpha \exp(-\varepsilon_\alpha/kT). \tag{44b}$$

In Liouville space notation, we write Eq. (43) in the form

$$|\rho(-\infty)\rangle\rangle = \sum_{a,\alpha} P(a)\rho_g(\alpha)\Big|{}^{a\alpha}_{a\alpha}\Big\rangle\rangle. \tag{45}$$

Here $|v\lambda\rangle\rangle$ is the Liouville space vector corresponding to $|v\rangle\langle\lambda|$. $\Big|{}^{a\alpha}_{a\alpha}\Big\rangle\rangle$ stands for the direct product of the system $|aa\rangle\rangle$ state and the bath $|\alpha\alpha\rangle\rangle$ state. For subsequent manipulations we further introduce the system and the bath density matrices corresponding to thermal equilibrium within the electronically excited state, that is,

$$\sigma_e = \exp(-H_e/kT)/\mathrm{Tr}\exp(-H_e/kT) = \sum_b |b\rangle P(b)\langle b|, \tag{46a}$$

$$\rho_e = \exp(-h_e/kT)/\mathrm{Tr}\exp(-h_e/kT) = \sum_\beta |\beta\rangle \rho_e(\beta)\langle\beta|, \tag{46b}$$

where the sums run over the excited-state manifold, and $P(b)$ and $\rho_e(\beta)$ are defined by Eqs. (44), by interchanging the indexes a and α to b and β, respectively. The electronic dipole operator of the absorber couples vibronic states belonging to different electronic states. We then have

$$V = \sum_{a,b,c,d} [\mu_{ab}|a\rangle\langle b| + \mu_{da}|d\rangle\langle a| + \mu_{cb}|c\rangle\langle b| + \mu_{dc}|d\rangle\langle c|], \quad (47)$$

where the summation runs over the entire manifolds of ground and electronically excited states. We are now in a position to calculate the nonlinear response function $R(t_3, t_2, t_1)$ [Eq. (29)] for the present model system. The radiative interaction $\Upsilon^{\times}$ is a commutator that can act either from the left or from the right, and its matrix elements are[11]

$$\langle\langle \nu'\lambda'|\Upsilon^{\times}|\nu\lambda\rangle\rangle = \mu_{\nu'\nu}\delta_{\lambda'\lambda} - \mu^{*}_{\lambda'\lambda}\delta_{\nu'\nu}. \quad (48)$$

The first and second terms in Eq. (48) correspond, respectively, to action of $\Upsilon^{\times}$ from the left and from the right. Since Eq. (29) contains three factors of the radiative interaction $\Upsilon^{\times}$, it will have $2^3 = 8$ terms corresponding to the various possible choices of the $\Upsilon^{\times}$s to act from the left or the right. A pictorial representation of Eq. (29) is given in Fig. 5. We start at $|\rho(-\infty)\rangle\rangle = |aa\rangle\rangle$,

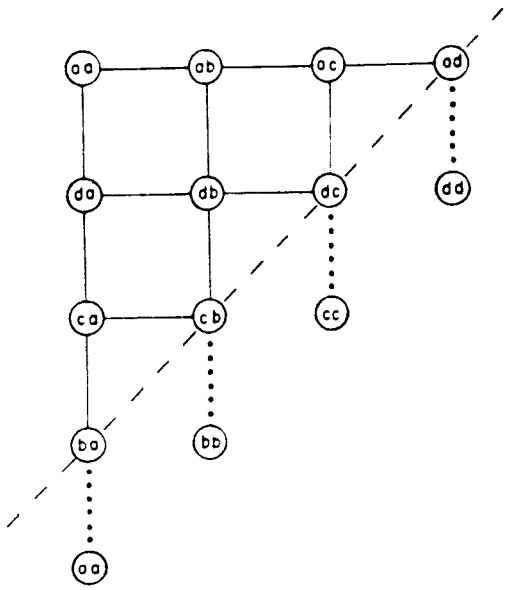

Figure 5. Pictoral representation of the Liouville space pathways that contribute to the nonlinear response function [Eqs. (49) and (53)]. Solid lines denote radiative coupling V, horizontal (vertical) lines represent action of V from the right (left). Starting at aa, after three perturbations, the system finds itself along the dashed line. The dotted lines represent the last V, which acts from the left. At the end of four perturbations, the system is in a diagonal state (aa, bb, cc, or dd). The number of three-bond pathways leading to ad, ba, dc, and cb is 1, 1, 3, and 3, respectively. Altogether, there are, therefore, eight pathways, which are shown in Fig. 6. In each pathway, each of the three incoming fields acts once.

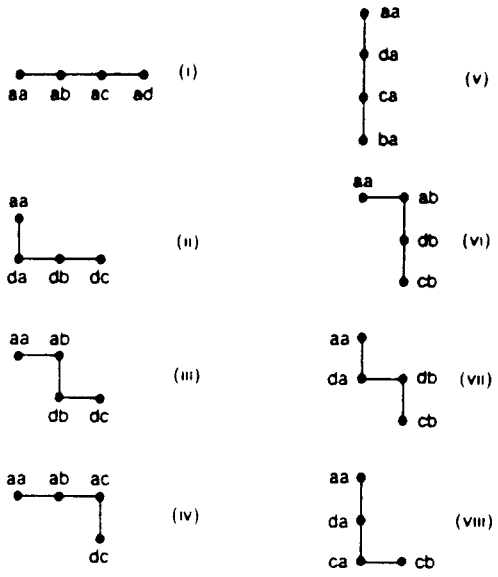

Figure 6. The eight Liouville space pathways that contribute to the nonlinear response function [Eq. (49) or (53)]. The eight terms in Eqs. (49), (53), (57), (60), and (63) correspond, respectively, to pathways (i)–(viii).

which is in the upper left corner. A horizontal (vertical) bond represents an interaction $\mathcal{V}$ acting from the right (left). After the first interaction (which takes place at time $t - t_1 - t_2 - t_3$) the system finds itself in either of the states $|ab\rangle\rangle$ or $|da\rangle\rangle$ (note that b and d are dummy indices that run over the entire excited-state manifold). The system then evolves for a period t_1, interacts again (at time $t - t_2 - t_3$), evolves for a period t_2, interacts again at time $t - t_3$, and evolves for a period t_3. Then, at time t the polarization is calculated by acting with V from the left and performing a trace. The eight pathways in Fig. 5 that contribute to R are displayed in Fig. 6. Making use of Eqs. (29), (41)–(43), (47), and (48), we obtain the nonlinear response function[6,19]

$$\begin{aligned} R(t_3,t_2,t_1) = \sum_{a,b,c,d} & P(a)\mu_{ab}\mu_{bc}\mu_{cd}\mu_{da} \\ & \times [-\langle G_{ad}(t_3)G_{ac}(t_2)G_{ab}(t_1)\rangle + \langle G_{dc}(t_3)G_{db}(t_2)G_{da}(t_1)\rangle \\ & + \langle G_{dc}(t_3)G_{db}(t_2)G_{ab}(t_1)\rangle + \langle G_{dc}(t_3)G_{ac}(t_2)G_{ab}(t_1)\rangle \\ & + \langle G_{ba}(t_3)G_{ca}(t_2)G_{da}(t_1)\rangle - \langle G_{cb}(t_3)G_{db}(t_2)G_{ab}(t_1)\rangle \\ & - \langle G_{cb}(t_3)G_{db}(t_2)G_{da}(t_1)\rangle - \langle G_{cb}(t_3)G_{ca}(t_2)G_{da}(t_1)\rangle], \end{aligned} \tag{49}$$

where the eight terms correspond to the pathways (i)–(viii) of Fig. 6, respectively.

The following notation was introduced in Eq. (49):

$$G_{\nu\lambda}(t) \equiv \langle\langle \nu\lambda | G(t) | \nu\lambda \rangle\rangle_S = \mathrm{Tr}_S[|\lambda\rangle\langle\nu|G(t)|\nu\rangle\langle\lambda|]. \tag{50}$$

The subscript S signifies that this is a matrix element in the system space only, that is, we perform a partial trace over the system degrees of freedom, and $G_{\nu\lambda}(t)$ is still a full Liouville space operator in the bath degrees of freedom. The angular brackets $\langle \cdots \rangle$ denote averaging over the bath degrees of freedom, that is,

$$\langle G \rangle = \sum_{\alpha,\alpha'} \langle\langle \alpha'\alpha' | G | \alpha\alpha \rangle\rangle \rho_g(\alpha). \tag{51}$$

This is the usual thermodynamic averaging, which amounts to averaging over initial states $|\alpha\alpha\rangle\rangle$ and summing over final states $|\alpha'\alpha'\rangle\rangle$. To clarify the notation, we shall write explicitly the first term in Eq. (49):

$$\begin{aligned}\langle G_{ad}(t_3) G_{ac}(t_2) G_{ab}(t_1) \rangle = \sum_{\alpha,\alpha_1,\alpha_2,\alpha_3,\alpha_4,\alpha'} & \langle\langle {}^{\alpha'\alpha'}_{\alpha d} | G(t_3) | {}^{\alpha_3\alpha_4}_{\alpha d} \rangle\rangle \langle\langle {}^{\alpha_3\alpha_4}_{\alpha c} | G(t_2) | {}^{\alpha_1\alpha_2}_{\alpha c} \rangle\rangle \\ & \times \langle\langle {}^{\alpha_1\alpha_2}_{\alpha b} | G(t_1) | {}^{\alpha\alpha}_{ab} \rangle\rangle \rho_g(\alpha).\end{aligned} \tag{52}$$

Alternatively, making use of Eq. (32), we obtain the nonlinear response function in the frequency domain:

$$\begin{aligned}&\hat{R}(\omega_1 - \omega_2 + \omega_3, \omega_1 - \omega_2, \omega_1) \\ &\quad = \sum_{a,b,c,d} P(a) \mu_{ab} \mu_{bc} \mu_{cd} \mu_{da} \\ &\qquad \times [- \langle \hat{G}_{ad}(\omega_1 - \omega_2 + \omega_3) \hat{G}_{ac}(\omega_1 - \omega_2) \hat{G}_{ab}(\omega_1) \rangle \\ &\qquad + \langle \hat{G}_{dc}(\omega_1 - \omega_2 + \omega_3) \hat{G}_{db}(\omega_1 - \omega_2) \hat{G}_{da}(\omega_1) \rangle \\ &\qquad + \langle \hat{G}_{dc}(\omega_1 - \omega_2 + \omega_3) \hat{G}_{db}(\omega_1 - \omega_2) \hat{G}_{ab}(\omega_1) \rangle \\ &\qquad + \langle \hat{G}_{dc}(\omega_1 - \omega_2 + \omega_3) \hat{G}_{ac}(\omega_1 - \omega_2) \hat{G}_{ab}(\omega_1) \rangle \\ &\qquad + \langle \hat{G}_{ba}(\omega_1 - \omega_2 + \omega_3) \hat{G}_{ca}(\omega_1 - \omega_2) \hat{G}_{da}(\omega_1) \rangle \\ &\qquad - \langle \hat{G}_{cb}(\omega_1 - \omega_2 + \omega_3) \hat{G}_{db}(\omega_1 - \omega_2) \hat{G}_{ab}(\omega_1) \rangle \\ &\qquad - \langle \hat{G}_{cb}(\omega_1 - \omega_2 + \omega_3) \hat{G}_{db}(\omega_1 - \omega_2) \hat{G}_{da}(\omega_1) \rangle \\ &\qquad - \langle \hat{G}_{cb}(\omega_1 - \omega_2 + \omega_3) \hat{G}_{ca}(\omega_1 - \omega_2) \hat{G}_{da}(\omega_1) \rangle].\end{aligned} \tag{53}$$

Here again, the eight terms correspond, respectively, to the pathways (i)–(viii) of Fig. 6. $\hat{G}_{\nu\lambda}(\omega)$ and the angular brackets $\langle \cdots \rangle$ are analogous to Eq. (51).

We note that the nonlinear response function $R(t_3,t_2,t_1)$ [Eq. (49)] or $\tilde{R}(\omega_1+\omega_2+\omega_3,\omega_1+\omega_2,\omega_1)$ [Eq. (53)] is the fundamental quantity that contains all the relevant microscopic information for any 4WM process. Ideal time-domain 4WM probes directly $|R(t_3,t_2,t_1)|^2$ [Eq. (36)]. The response function contains eight terms that correspond to the eight distinct pathways in Liouville space (Fig. 6). Frequency-domain 4WM is described by $\chi^{(3)}$ [Eq. (40)], which has $6\times 8=48$ terms corresponding to the $3!=6$ permutations of the time ordering of the three fields that can be made for each of the eight pathways. In time-domain 4WM we have fewer terms than in frequency-domain 4WM, since in the former we can control the relative order in time of the interactions with the three fields, whereas in the latter all orderings contribute equally to the signal. The Liouville space notation used in this section is useful, since it allows us to follow the time evolution of the density matrix. It will further allow us to introduce the factorization approximation in Section IV. Before doing that, however, we note that we can express Eq. (49) in terms of ordinary (not Liouville) operators. To that end we introduce the four-point correlation function of the dipole operator,[19,57] that is,

$$\begin{aligned} F(\tau_1,\tau_2,\tau_3,\tau_4) &= \mathrm{Tr}[V(\tau_1)V(\tau_2)V(\tau_3)V(\tau_4)\rho(-\infty)] \\ &= \langle V(\tau_1)V(\tau_2)V(\tau_3)V(\tau_4)\rangle, \end{aligned} \tag{54}$$

where

$$V(\tau)=\exp(iH\tau)V\exp(-iH\tau). \tag{55}$$

Here H is the molecular Hamiltonian [Eq. (41)] and V is the dipole operator [Eq. (47)]. In terms of the system and the bath eigenstates [Eqs. (42)], we can recast Eq. (54) in the form

$$\begin{aligned} F(\tau_1,\tau_2,\tau_3,\tau_4) = \sum_{\substack{a,b,c,d \\ \alpha,\alpha_1,\alpha_2,\alpha_3}} & \langle a\alpha|V(\tau_1)|d\alpha_3\rangle\langle d\alpha_3|V(\tau_2)|c\alpha_2\rangle\langle c\alpha_2|V(\tau_3)|b\alpha_1\rangle \\ & \times\langle b\alpha_1|V(\tau_4)|a\alpha\rangle P(a)\rho_g(\alpha) \end{aligned} \tag{56}$$

In terms of this four-point correlation function, we have[6,19]

$$\begin{aligned} R(t_3,t_2,t_1) = & -F(0,t_1,t_1+t_2,t_1+t_2+t_3)+F(t_1,t_1+t_2,t_1+t_2+t_3,0) \\ & +F(0,t_1+t_2,t_1+t_2+t_3,t_1)+F(0,t_1,t_1+t_2+t_3,t_1+t_2) \\ & +F(t_1+t_2+t_3,t_1+t_2,t_1,0)-F(0,t_1+t_2+t_3,t_1+t_2,t_1) \\ & -F(t_1,t_1+t_2+t_3,t_1+t_2,0)-F(t_1+t_2,t_1+t_2+t_3,t_1,0), \end{aligned} \tag{57}$$

where the eight terms correspond, respectively, to pathways (i)–(viii) of Fig. 6. It is therefore clear that the various 4WM processes probe different features of the four-point correlation function of the dipole operator. The response function discussed in this article is closely related to that introduced by Butcher.[2] Our time arguments t_1, t_2, and t_3 (Fig. 3) were chosen differently. With the present choice, the relations between time-domain and frequency-domain experiments is more transparent. Since the response function is probing the four-point correlation function [Eq. (54)], it necessarily contains more information than the ordinary absorption lineshape, which is given by the two-time correlation function $\langle V(\tau)V(0)\rangle$.[11] This can be utilized, for example, to eliminate selectively inhomogeneous broadening as is done in photon echoes.[22-25,43] Specific applications to coherent Raman spectroscopy and approximate schemes for the evaluation of the nonlinear response function will be developed in the subsequent sections.

IV. THE FACTORIZATION APPROXIMATION

Equations (49), (53), and (57) provide rigorous correlation function expressions for the nonlinear response function. In general, in order to calculate the spectral lineshapes in nonlinear optical processes, we need to solve for the correlated dynamics of the system and of the bath degrees of freedom. In this section, we shall develop an approximate expression for the nonlinear response function, which is based on the assumption of separation of time scales between the system and the bath. Under very general conditions, which will be precisely specified, it is possible to factorize the average of the product of Liouville space operators into a product of averages. This results in a considerable simplification of the final expressions and provides a useful method of modeling realistic molecules in solutions.[11,19,64] Let us examine Eq. (52) in more detail (see Fig. 6). During the time period t_1, the system is in an optical coherence $|a\rangle\langle b|$ between the ground and electronically excited states. The bath, which was initially in thermal equilibrium with the system in the ground electronic state, is now interacting with the system and undergoes a time evolution. Its state at the end of the t_1 period is $|\alpha_1\rangle\langle\alpha_2|$. Then a second radiative interaction takes place, and the system returns to the ground electronic state ($|a\rangle\langle c|$ is a part of the ground-state manifold $|g\rangle\langle g|$). During the t_2 period, the bath (which is now in a nonequilibrium state) changes its state to $|\alpha_3\rangle\langle\alpha_4|$. The relevant duration of the t_2 period is of the order of the lifetime of the vibronic states $|a\rangle$ and $|c\rangle$. This time is expected to be much longer than a typical solvent relaxation time (10^{-13} sec), which restores the solvent to equilibrium with the $|g\rangle\langle g|$ system state. Therefore, after a very short time (much shorter than a typical value of t_2), the bath returns to the ρ_g distribution. We can therefore assume that at the beginning and at the end of the t_2 period the bath is in thermal equilibrium and its density matrix is ρ_g.

Then a third radiative interaction occurs. The system returns to an optical coherence, $|a\rangle\langle d|$, and evolves with the bath for a period t_3. This description is appropriate for pathways (i), (iv), (v). (viii) of Eq. (49). For the other pathways [(ii), (iii), (vi), and (vii)], there is one difference. During the period t_2 the system is in the excited electronic state $|e\rangle\langle e|$ (rather than in $|g\rangle\langle g|$). We then expect the bath to relax rapidly to the new equilibrium ρ_e [Eq. (46b)] rather than ρ_g. This is the solvent reorganization process.[65] During the period t_2 in these pathways, the state of the bath can therefore be assumed to be ρ_e.

These considerations suggest the introduction of the following projection operator[59,64]:

$$\hat{P} = |gg\rangle\!\rangle\langle\!\langle gg|\rho_g \mathrm{Tr}_B + |ee\rangle\!\rangle\langle\!\langle ee|\rho_e \mathrm{Tr}_B, \tag{58a}$$

or, alternatively,

$$\hat{P} = \sum_{\alpha,\alpha'} \rho_g(\alpha)|^{\alpha\alpha}_{gg}\rangle\!\rangle\langle\!\langle^{\alpha'\alpha'}_{g\,g}| + \sum_{\beta,\beta'} \rho_e(\beta)|^{\beta\beta}_{ee}\rangle\!\rangle\langle\!\langle^{\beta'\beta'}_{e\,e}|. \tag{58b}$$

The factorization approximation may now be introduced by substituting into Eq. (49):

$$G(t_2) \to \hat{P}G(t_2)\hat{P}. \tag{59}$$

This projection operator replaces the bath distribution at the end of the t_2 period by ρ_g if the system is in the ground electronic state, and by ρ_e if the system is electronically excited. Making use of Eq. (59), Eq. (49) assumes the form[19]

$$\begin{aligned} R(t_3,t_2,t_1) &= \sum_{a,b,c,d} P(a)\mu_{ab}\mu_{bc}\mu_{cd}\mu_{da}[-I_{ad}(t_3)I_{ac}(t_2)I_{ab}(t_1)J_g^*(t_3)J_g^*(t_1) \\ &+ I_{dc}(t_3)I_{db}(t_2)I_{da}(t_1)J_e^*(t_3)J_g(t_1) + I_{dc}(t_3)I_{db}(t_2)I_{ab}(t_1)J_e^*(t_3)J_g^*(t_1) \\ &+ I_{dc}(t_3)I_{ac}(t_2)I_{ab}(t_1)J_g(t_3)J_g^*(t_1) + I_{ba}(t_3)I_{ca}(t_2)I_{da}(t_1)J_g(t_3)J_g(t_1) \\ &- I_{cb}(t_3)I_{db}(t_2)I_{ab}(t_1)J_e(t_3)J_g^*(t_1) - I_{cb}(t_3)I_{db}(t_2)I_{da}(t_1)J_e(t_3)J_g(t_1) \\ &- I_{cb}(t_3)I_{ca}(t_2)I_{da}(t_1)J_g^*(t_3)J_g(t_1)]. \end{aligned} \tag{60}$$

Here,

$$I_{\nu\lambda}(t) = \exp[-i\omega_{\nu\lambda}t - \Gamma_{\nu\lambda}|t|], \tag{61a}$$

where

$$\omega_{\nu\lambda} \equiv \varepsilon_\nu - \varepsilon_\lambda \tag{61b}$$

and

$$\Gamma_{\nu\lambda} \equiv \tfrac{1}{2}(\gamma_\nu + \gamma_\lambda). \tag{61c}$$

γ_ν^{-1} is the lifetime of level $|\nu\rangle$, which is introduced here phenomenologically. A more detailed discussion of lifetimes and relaxation is given in Sec. VIII. $I_{\nu\lambda}(t)$ represents the system contribution to the correlation function. The entire effect of the bath, in this case, is contained in the line broadening functions $J_g(t)$ and $J_e(t)$, defined as follows[64]:

$$J_g(t) = \mathrm{Tr}_B[\exp(ih_g t)\exp(-ih_e t)\rho_g] \tag{62a}$$

and

$$J_e(t) = \mathrm{Tr}_B[\exp(ih_e t)\exp(-ih_g t)\rho_e]. \tag{62b}$$

Here Tr_B stands for a trace over the bath degrees of freedom. $J_g(t)$ represents the dephasing effects resulting from thermal fluctuations of the bath, when the bath is equilibrated with the system in the ground electronic state, and its density matrix is ρ_g. $J_e(t)$ represents the same effects when the bath is equilibrated with the system in the electronically excited state $|e\rangle$ (i.e., after the solvent reorganization takes place), and its density matrix is ρ_e. All pathways contain $J_g(t_1)$, since the system is initially in the ground state. Pathways (i), (iv), (v), and (viii) contain $J_g(t_3)$, since during t_2 the bath is equilibrated with the ground-state system; whereas the other pathways contain $J_e(t_3)$, since during the t_2 interval the bath has relaxed to its new equilibrium with the system being excited. Upon the substitution of Eq. (60) into Eq. (30), we obtain the response function in the frequency domain:

$$\begin{aligned}
&\hat{R}(\omega_1 - \omega_2 + \omega_3, \omega_1 - \omega_2, \omega_1) \\
&\quad = \sum_{a,b,c,d} P(a)\mu_{ab}\mu_{bc}\mu_{cd}\mu_{da} \\
&\qquad \times \left[-\frac{I_{da}^*(-\omega_1 + \omega_2 - \omega_3)I_{ba}^*(-\omega_1)}{\omega_1 - \omega_2 - \omega_{ac} + i\Gamma_{ac}} + \frac{\bar{I}_{dc}(\omega_1 - \omega_2 + \omega_3)I_{da}(\omega_1)}{\omega_1 - \omega_2 - \omega_{db} + i\Gamma_{db}} \right. \\
&\qquad - \frac{\bar{I}_{dc}(\omega_1 - \omega_2 + \omega_3)I_{ba}^*(-\omega_1)}{\omega_1 - \omega_2 - \omega_{db} + i\Gamma_{db}} - \frac{I_{dc}(\omega_1 - \omega_2 + \omega_3)I_{ba}^*(-\omega_1)}{\omega_1 - \omega_2 - \omega_{ac} + i\Gamma_{ac}} \\
&\qquad + \frac{I_{ba}(\omega_1 - \omega_2 + \omega_3)I_{da}(\omega_1)}{\omega_1 - \omega_2 - \omega_{ca} + i\Gamma_{ac}} - \frac{\bar{I}_{bc}^*(-\omega_1 + \omega_2 - \omega_3)I_{ba}^*(-\omega_1)}{\omega_1 - \omega_2 - \omega_{db} + i\Gamma_{db}} \\
&\qquad \left. + \frac{\bar{I}_{bc}^*(-\omega_1 + \omega_2 - \omega_3)I_{da}(\omega_1)}{\omega_1 - \omega_2 - \omega_{db} + i\Gamma_{db}} + \frac{I_{bc}^*(-\omega_1 + \omega_2 - \omega_3)I_{da}(\omega_1)}{\omega_1 - \omega_2 - \omega_{ca} + i\Gamma_{ac}} \right].
\end{aligned} \tag{63}$$

Here the complex lineshape functions I and $\bar{I}$ are given by

$$I_{\nu\lambda}(\omega) = -i\int_0^\infty d\tau\, I_{\nu\lambda}(\tau)J_g(\tau)\exp(i\omega\tau) \tag{64a}$$

and

$$\bar{I}_{\nu\lambda}(\omega) = -i\int_0^\infty d\tau\, I_{\nu\lambda}(\tau)J_e^*(\tau)\exp(i\omega\tau). \tag{64b}$$

$I_{\nu\lambda}(\omega)$ represents an absorption lineshape broadened by $J_g(\tau)$, whereas $\bar{I}_{\nu\lambda}(\omega)$ represents an emission lineshape broadened by $J_e^*(\tau)$.

V. CORRELATION FUNCTIONS FOR SPONTANEOUS RAMAN AND FLUORESCENCE LINESHAPES

In the previous sections, we derived general correlation function expressions for the nonlinear response function that allow us to calculate any 4WM process. The final results were recast as a product of Liouville space operators [Eqs. (49) and (53)], or in terms of the four-time correlation function of the dipole operator [Eq. (57)]. We then developed the factorization approximation [Eqs. (60) and (63)], which simplifies these expressions considerably. In this section, we shall consider the problem of spontaneous Raman and fluorescence spectroscopy. General formal expressions analogous to those obtained for 4WM will be derived. This will enable us to treat both experiments in a similar fashion and compare their information content. We shall start with the ordinary absorption lineshape. Consider our system interacting with a stationary monochromatic electromagnetic field with frequency ω. The total initial density matrix is given by

$$|\rho(-\infty)\rangle\rangle = |\rho_S(-\infty)\rangle\rangle|\rho_B(-\infty)\rangle\rangle|\rho_R(-\infty)\rangle\rangle, \tag{65}$$

where the system and the bath are in thermal equilibrium, and the incident field has n photons in the incoming mode, that is,

$$|\rho_R(-\infty)\rangle\rangle = |n,n\rangle\rangle. \tag{66}$$

In an absorption experiment, we measure the steady-state rate of change of the occupation number of this mode. The operator representing this quantity is

$$B = \frac{d}{dt}a_1^\dagger a_1 = iL_{\text{int}}a_1^\dagger a_1 = i[H_{\text{int}}, a_1^\dagger a_1]. \tag{67}$$

The absorption lineshape $\sigma(\omega)$ is given by the linear response to the stationary external field. To that end, we need to evaluate the density matrix to first order in L_{int}. We then have

$$\sigma(\omega) = \langle\langle B|\rho^{(1)}\rangle\rangle. \tag{68}$$

Making use of Eqs. (67) and (68), and eliminating some numerical constants, we obtain

$$\sigma(\omega) = (-i)^2 \int_0^\infty dt \langle\langle a_1^\dagger a_1 | \hat{\mathcal{V}} G(t) \hat{\mathcal{V}} | \rho(-\infty)\rangle\rangle \exp(i\omega t) \tag{69a}$$

or

$$\sigma(\omega) = -i\langle\langle a_1^\dagger a_1 | \hat{\mathcal{V}} \hat{G}(\omega) \hat{\mathcal{V}} | \rho(-\infty)\rangle\rangle. \tag{69b}$$

Equation (69b) can be recast in the form

$$\sigma(\omega) = -2\,\text{Im} \sum_{a,b} P(a)|\mu_{ab}|^2 \langle \hat{G}_{ba}(\omega)\rangle. \tag{70}$$

We next turn to the spontaneous Raman and fluorescence lineshapes. In an SRF experiment, we have a single incident classical field (ω_1) and a single scattered mode (ω_2). We shall use the Hamiltonian [Eq. (2)] with the only difference that the sum in Eq. (4) runs over $j = 1, 2$, with E_1 being the classical incident field and E_2 being the scattered field, which will be treated quantum mechanically. In an SRF experiment, we monitor the scattered field with both time and frequency resolution. The operator representing the rate of emission of ω_2 photons is

$$B = \frac{d}{dt}a_2^\dagger a_2 = iL_{\text{int}}a_2^\dagger a_2 = i[H_{\text{int}}, a_2^\dagger a_2]. \tag{71}$$

The observed rate of photon emission is

$$S'(\omega_1, \omega_2, t) = \langle\langle B|\rho(t)\rangle\rangle. \tag{72}$$

$\rho(t)$ will now be evaluated using third-order perturbation theory, resulting in

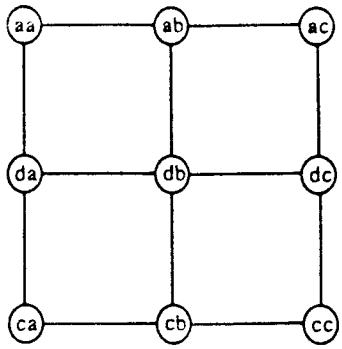

Figure 7. Pictorial representation of the pathways in Liouville space that contribute to SRF spectra. Solid lines denote radiative coupling V. Horizontal (vertical) lines represent action of V from the right (left). The SRF process is obtained by all pathways that start at aa and end at cc in fourth order (four bonds). There are six pathways that contribute. However, owing to symmetry, we need consider only the three pathways shown in Fig. 8. The other three are obtained by a complex conjugation and permutation of b and d.

$$S'(\omega_1,\omega_2,t)=\int_0^\infty dt_1\int_0^\infty dt_2\int_0^\infty dt_3\langle\langle a_2^\dagger a_2|L_{\rm int}(t)G(t_3)L_{\rm int}(t-t_3)$$
$$\times G(t_2)L_{\rm int}(t-t_2-t_3)G(t_1)L_{\rm int}(t-t_1-t_2-t_3)|\rho(-\infty)\rangle\rangle. \tag{73}$$

When Eq. (73) is explicitly evaluated, we find that within the rotating wave approximation we need to calculate six pathways (Fig. 7). The contribution of three of them is the complex conjugate of the others. We therefore need to consider only the three pathways shown in Fig. 8. We then get[11,12,57,64]

$$S'(\omega_1,\omega_2,t)=2\,\mathrm{Re}\sum_{a,b,c,d}P(a)\mu_{ab}\mu_{bc}\mu_{cd}\mu_{da}\int_0^\infty dt_1\int_0^\infty dt_2\int_0^\infty dt_3$$
$$\times\{\langle G_{cb}(t_3)G_{db}(t_2)G_{ab}(t_1)\rangle\exp[-i\omega_2t_3-i\omega_1t_1]$$
$$\times E^*(t-t_1-t_2-t_3)E(t-t_2-t_3)$$
$$+\langle G_{dc}(t_3)G_{db}(t_2)G_{ab}(t_1)\rangle\exp[i\omega_2t_3-i\omega_1t_1]$$
$$\times E^*(t-t_1-t_2-t_3)E(t-t_2-t_3)$$
$$+\langle G_{dc}(t_3)G_{ac}(t_2)G_{ab}(t_1)\rangle\exp[i\omega_2t_3-i(\omega_1-\omega_2)t_2-i\omega_1t_1]$$
$$\times E^*(t-t_1-t_2-t_3)E(t-t_3)\}, \tag{74}$$

where the notation is identical to that of Eq. (49). The three terms in Eq. (74) correspond, respectively, to pathways (i)–(iii) of Fig. 8. In a steady-state

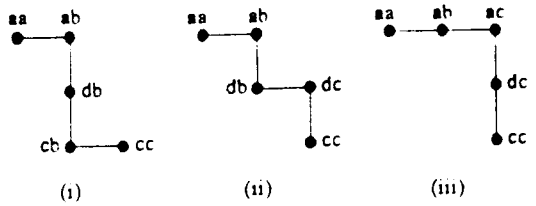

Figure 8. The three Liouville space pathways that contribute to SRF spectra. The three terms in each of Eqs. (74)–(78) correspond, respectively, to pathways (i), (ii), and (iii).

experiment, $E(\tau)$ is independent of τ. Setting $E(\tau) = E$ in Eq. (74) results in the following expression for steady-state SRF[64]:

$$S_{SRF}(\omega_1,\omega_2) = 2\,\mathrm{Im}\sum_{a,b,c,d} P(a)\mu_{ab}\mu_{bc}\mu_{cd}\mu_{da}[\langle \hat{G}_{cb}(-\omega_2)\hat{G}_{db}(0)\hat{G}_{ab}(-\omega_1)\rangle + \langle \hat{G}_{dc}(\omega_2)\hat{G}_{db}(0)\hat{G}_{ab}(-\omega_1)\rangle + \langle \hat{G}_{dc}(\omega_2)\hat{G}_{ac}(\omega_2-\omega_1)\hat{G}_{ab}(-\omega_1)\rangle]. \tag{75}$$

In pathways (i) and (ii), the system first interacts twice with the ω_1 field at times $t - t_1 - t_2 - t_3$ and $t - t_2 - t_3$ and then twice with the ω_2 mode at times $t - t_3$ and t. In pathway (iii), the system first interacts with ω_1 at time $t - t_1 - t_2 - t_3$, then, at time $t - t_2 - t_3$, it interacts with ω_2; then, at time $t - t_3$, it interacts again with ω_1, and finally, at time t, it interacts with ω_2. It also should be noted that the steady-state rate [Eq. (75)] is closely related to $\mathrm{Im}\,\chi^{(3)}(-\omega_2,\omega_2,-\omega_1,\omega_1)$. All the terms appearing in Eq. (75) appear also in $\chi^{(3)}$. However, $\chi^{(3)}$ contains more terms, which do not contribute to spontaneous emission, due to the quantum nature of ω_2. In analogy to Section IV, we can further recast Eq. (75) using the four-point correlation function of the dipole operator [Eq. (54)] resulting in[11,12,64]

$$\begin{aligned} S'(\omega_1,\omega_2,t) = 2\,\mathrm{Re}\int_0^\infty dt_1\int_0^\infty dt_2\int_0^\infty dt_3\{&F(0,t_1+t_2+t_3,t_1+t_2,t_1)\\ &\times \exp[-i\omega_2 t_3 - i\omega_1 t_1]E^*(t-t_1-t_2-t_3)E(t-t_2-t_3)\\ &+ F(0,t_1+t_2,t_1+t_2+t_3,t_1)\\ &\times \exp[i\omega_2 t_3 - i\omega_1 t_1]E^*(t-t_1-t_2-t_3)E(t-t_2-t_3)\\ &+ F(0,t_1,t_1+t_2+t_3,t_1+t_2)\\ &\times \exp[i\omega_2 t_3 - i(\omega_1-\omega_2)t_2 - i\omega_1 t_1]\\ &\times E^*(t-t_1-t_2-t_3)E(t-t_3)\}. \end{aligned} \tag{76}$$

Here the three terms correspond, respectively, to the three terms of Eq. (75). Finally, let us consider the factorization approximation. In pathways (i) and (ii), the system is in the excited state during the t_2 interval, whereas in pathways (iii), it is in the gound state. Introducing the projection operator [Eq. (59)] in Eq. (74) results in[64]

$$\begin{aligned} S'(\omega_1,\omega_2,t) = 2\,\mathrm{Re}\sum_{a,b,c,d} P(a)\mu_{ab}\mu_{bc}\mu_{cd}\mu_{da}\int_0^\infty dt_1\int_0^\infty dt_2\int_0^\infty dt_3 \\ \{I_{cb}(t_3)I_{db}(t_2)I_{ab}(t_1)J_e(t_3)J_g^*(t_1)\exp(-i\omega_2 t_3 - i\omega_1 t_1) \\ \times E^*(t-t_1-t_2-t_3)E(t-t_2-t_3) \\ + I_{dc}(t_3)I_{db}(t_2)I_{ab}(t_1)J_e^*(t_3)J_g^*(t_1)\exp[i\omega_2 t_3 - i\omega_1 t_1] \\ \times E^*(t-t_1-t_2-t_3)E(t-t_2-t_3) \\ + I_{dc}(t_3)I_{ac}(t_2)I_{ab}(t_1)J_g(t_3)J_g^*(t_1) \\ \times \exp[i\omega_2 t_3 - i(\omega_1-\omega_2)t_2 - i\omega_1 t_1] \\ \times E^*(t-t_1-t_2-t_3)E(t-t_3)\}. \end{aligned} \tag{77}$$

For steady-state experiments we take $E(t)$ in Eq. (77) to be independent of t, and we get

$$\begin{aligned} S_{\mathrm{SRF}}(\omega_1,\omega_2) \\ = 2\,\mathrm{Im}\sum_{a,b,c,d} P(a)\mu_{ab}\mu_{bc}\mu_{cd}\mu_{da} \\ \times\left(\frac{\bar{I}_{bc}^*(\omega_2)I_{ba}^*(\omega_1)}{\omega_{bd}+i\Gamma_{bd}} - \frac{\bar{I}_{dc}(\omega_2)I_{ba}^*(\omega_1)}{\omega_{bd}+i\Gamma_{bd}} - \frac{I_{dc}(\omega_2)I_{ba}^*(\omega_1)}{\omega_2-\omega_1-\omega_{ac}+i\Gamma_{ac}}\right). \end{aligned} \tag{78}$$

In conclusion, in this section we presented the formal expressions for the absorption lineshape [Eq. (70)] and for spontaneous Raman and fluorescence spectroscopy. For the latter, we derived Liouville space expressions in the time and the frequency domain [Eqs. (74) and (75)], an ordinary correlation function expression [Eq. (76)], and, finally, the factorization approximation resulted in Eqs. (77) and (78). The factorization approximation is expected to hold in many cases for steady-state experiments and for time-resolved experiments with low temporal resolution. It is possible to observe a time-dependent shift of spontaneous emission lineshapes using picosecond excitation and detection [66–68]. This shift arises from the reorganization process of the solvent and also from vibrational relaxation that occurs during the t_2 time interval. A proper treatment of these effects requires going beyond the

present factorization approximation, which assumes an instantaneous reorganization. Our formalism is ideally suited for developing microscopic models for the solvent reorganization and incorporating them properly in $G(t_2)$. We have recently developed such a theory by introducing a solvation coordinate. The theory is based on a factorization approximation for all the solvent degrees of freedom, except for the solvation coordinate whose dynamics is related to the dielectric properties of the solvent.[68] Some calculations of time-dependent fluorescence lineshapes will be presented in Sec. VIII, following the introduction of the vibrational relaxation processes, which constitute another factor contributing to these lineshapes.

VI. NONLINEAR OPTICS OF POLYATOMIC HARMONIC MOLECULES IN CONDENSED PHASES—"EIGENSTATE-FREE" SPECTROSCOPY

The expressions developed in Sections IV and V for the nonlinear response function and for the SRF lineshape include four summations over molecular states (a, b, c, d). These summations can be carried out easily for small molecules with a few relevant levels. However, for large polyatomic molecules, they become intractable. In this section, we recast the previous expressions in terms of generalized molecular polarizabilities. This allows us to formally eliminate two of the four summations. For a simple, but realistic, model of harmonic molecules, it is possible to evaluate these polarizabilities using Green's function Fourier-transform techniques.[12,44,45,58] We thus end up with a closed expression most suitable for numerical computations, both in the time domain $[R(t_3, t_2, t_1)]$ and in the frequency domain $[\hat{R}(\omega_1 - \omega_2 + \omega_3, \omega_1 - \omega_2, \omega_1)]$. The time-domain formula can be simplified even further for this model by carrying out all four summations, resulting in an explicit expression for $R(t_3, t_2, t_1)$ in which all the summations have been eliminated. This formula,[45] which is particularly useful for time-domain 4WM, will be developed in Section X [Eq. (133)]. The transformation to the frequency domain is, however, more complex in this case, and the calculation of $\hat{R}(\omega_1 - \omega_2 + \omega_3, \omega_1 - \omega_2, \omega_1)$ via Eq. (30) requires the performing of a triple Fourier transform (rather than the single Fourier transforms required in this section). For simplicity, we hereafter assume that the lifetimes of electronically excited vibronic states are the same, that is, $\gamma_b = \gamma_d = \gamma$, and that for the ground electronic state $\gamma_a = \gamma_c = \gamma'$. We shall now introduce the following operators[64]:

$$T(t) = V \exp(-iH_e t - \gamma' t/2) V J_g(t), \tag{79a}$$

$$\tilde{T}(t) = V \exp(-iH_g t - \gamma t/2) V J_e(t), \tag{79b}$$

$$\tilde{T}(t) = V\sigma_g \exp(-iH_g t - \gamma t/2) V J_g^*(t), \tag{79c}$$

We further introduce the ground-state partition function

$$Z = \mathrm{Tr}_S \exp(-H_g/kT). \tag{79d}$$

Equation (60) can then be written in the form[45]

$$\begin{aligned} R(t_3,t_2,t_1) = \sum_{a,c} P(a)\{ & -T^*_{ac}(t_3)I_{ac}(t_2)T^*_{ca}(t_1)\exp[-i\varepsilon_a t_3 - i\varepsilon_a t_1] \\ & + T_{ca}(t_3)I_{ac}(t_2)T^*_{ca}(t_1)\exp[i\varepsilon_c t_3 - i\varepsilon_a t_1] \\ & + T_{ac}(t_3)I_{ca}(t_2)T_{ca}(t_1)\exp[i\varepsilon_a t_3 + i\varepsilon_a t_1] \\ & - T^*_{ca}(t_3)I_{ca}(t_2)T_{ca}(t_1)\exp[-i\varepsilon_c t_3 + i\varepsilon_a t_1]\} \\ & + \sum_{b,d}\{\bar{T}^*_{db}(t_3)I_{db}(t_2)\bar{T}^*_{bd}(t_1)\exp[-i\varepsilon_d t_3 - i\varepsilon_d t_1] \\ & + \bar{T}^*_{db}(t_3)I_{db}(t_2)\bar{T}_{db}(t_1)\exp[-i\varepsilon_d t_3 + i\varepsilon_b t_1] \\ & - \bar{T}_{bd}(t_3)I_{db}(t_2)\bar{T}_{db}(t_1)\exp[i\varepsilon_b t_3 + i\varepsilon_b t_1] \\ & - \bar{T}_{bd}(t_3)I_{db}(t_2)\bar{T}^*_{bd}(t_1)\exp[i\varepsilon_b t_3 - i\varepsilon_d t_1]\}. \end{aligned} \tag{80}$$

Upon the substitution of Eq. (80) into Eq. (30), we obtain the response function in the frequency domain. To that end, we introduce the following definitions:

$$K(\omega) = -i\int_0^\infty d\tau \exp(i\omega\tau)T(\tau), \tag{81a}$$

$$\bar{K}(\omega) = -i\int_0^\infty d\tau \exp(i\omega\tau)\bar{T}(\tau), \tag{81b}$$

$$\bar{\bar{K}}(\omega) = -i\int_0^\infty d\tau \exp(i\omega\tau)\bar{\bar{T}}(\tau), \tag{81c}$$

We then have

$$\begin{aligned} \hat{R}(\omega_1 - \omega_2 + \omega_3, \omega_1 - \omega_2, \omega_1) & \\ = \sum_{a,c} P(a)\Bigg(& -\frac{K^*_{ac}(\varepsilon_a - \omega_1 + \omega_2 - \omega_3)K^*_{ca}(\varepsilon_a - \omega_1)}{\omega_1 - \omega_2 - \omega_{ac} + i\Gamma_{ac}} \\ & - \frac{K_{ca}(\varepsilon_c + \omega_1 - \omega_2 + \omega_3)K^*_{ca}(\varepsilon_a - \omega_1)}{\omega_1 - \omega_2 - \omega_{ac} + i\Gamma_{ac}} \\ & + \frac{K_{ac}(\varepsilon_a + \omega_1 - \omega_2 + \omega_3)K_{ca}(\varepsilon_a + \omega_1)}{\omega_1 - \omega_2 - \omega_{ca} + i\Gamma_{ca}} \end{aligned}$$

$$+\frac{K^*_{ca}(\varepsilon_c-\omega_1+\omega_2-\omega_3)K_{ca}(\varepsilon_a+\omega_1)}{\omega_1-\omega_2-\omega_{ca}+i\Gamma_{ca}}\Bigg)$$

$$+\sum_{b,d}\Bigg(\frac{\bar{K}^*_{db}(\varepsilon_d-\omega_1+\omega_2-\omega_3)\bar{K}^*_{bd}(\varepsilon_d-\omega_1)}{\omega_1-\omega_2-\omega_{db}+i\Gamma_{db}}$$

$$-\frac{\bar{K}^*_{db}(\varepsilon_d-\omega_1+\omega_2-\omega_3)\bar{K}^*_{db}(\varepsilon_b-\omega_1)}{\omega_1-\omega_2-\omega_{db}+i\Gamma_{db}}$$

$$-\frac{\bar{K}_{bd}(\varepsilon_b+\omega_1-\omega_2+\omega_3)\bar{K}_{db}(\varepsilon_b+\omega_1)}{\omega_1-\omega_2-\omega_{db}+i\Gamma_{db}}$$

$$+\frac{\bar{K}_{bd}(\varepsilon_b+\omega_1-\omega_2+\omega_3)\bar{K}^*_{bd}(\varepsilon_d-\omega_1)}{\omega_1-\omega_2-\omega_{db}+i\Gamma_{db}}\Bigg). \tag{82}$$

Similarly, the absorption lineshape [Eq. (70)] can be recast in the form

$$\sigma(\omega)=-2\,\mathrm{Im}\sum_a P(a)K_{aa}(\varepsilon_a+\omega). \tag{83}$$

For the SRF lineshapes [Eq. (78)], we have

$$S_{\mathrm{SRF}}(\omega_1,\omega_2)=2\,\mathrm{Im}\Bigg(\sum_{b,d}\frac{[\bar{K}_{bd}(\varepsilon_b-\omega_2)-\bar{K}^*_{db}(\varepsilon_d-\omega_2)]\bar{K}_{db}(\varepsilon_b-\omega_1)}{\omega_{bd}+i\Gamma_{bd}}$$

$$-\sum_{a,c}P(a)\frac{K_{ca}(\varepsilon_c+\omega_2)K^*_{ca}(\varepsilon_a+\omega_1)}{\omega_2-\omega_1+\omega_{ca}+i\Gamma_{ca}}\Bigg). \tag{84}$$

The expressions derived in Sections IV and V explicitly contain four summations over molecular states (over a, b, c, and d). In Eqs. (80), (82), and (84), these summations have been rearranged, so that only two summations appear explicitly (either over a, c or over b, d). The other summations are "buried" in the definitions of $T(t)$, $\bar{T}(t)$, and $\bar{\bar{T}}(t)$ [Eq. (79)]. A significant reduction in computational effort may therefore be achieved if we can find an "eigenstate-free" procedure for the evaluation of the matrix elements of $T(t)$, $\bar{T}(t)$, and $\bar{\bar{T}}(t)$ without performing any summations. This may be done for a specific model of harmonic molecules, which will now be introduced. Consider a polyatomic harmonic molecule with N vibrational modes. Its Hamiltonian is

$$H=|g\rangle H_g\langle g|+|e\rangle[\omega_{eg}+H_e-i\gamma/2]\langle e|, \tag{85a}$$

with

$$H_g = \frac{1}{2}\sum_{j=1}^{N} \omega_j''(p_j''^2 + q_j''^2 - 1), \tag{85b}$$

$$H_e = \frac{1}{2}\sum_{j=1}^{N} \omega_j'(p_j'^2 + q_j'^2 - 1) \tag{85c}$$

and

$$p_j' = \left(\frac{1}{m_j\omega_j'\hbar}\right)^{1/2} P_j', \tag{86}$$

$$q_j' = \left(\frac{m_j\omega_j'}{\hbar}\right)^{1/2} Q_j'. \tag{87}$$

We adopt here the common spectroscopic notation and use a superscript double prime and prime to denote quantities belonging to the ground and to the electronically excited states, respectively. P_j' and Q_j' are the conjugate momentum and the normal coordinate of the jth mode of the excited state. The transformation [Eqs. (86) and (87)] defines p_j' and q_j', which are the dimensionless momentum and normal coordinate of the jth mode. A similar transformation between p_j'', q_j'', and P_j'', Q_j'' is defined by changing all prime indexes in Eqs. (86) and (87) to double primes. $\omega_j'(\omega_j'')$ and m_j are the frequency and the mass of the jth mode. The present Hamiltonian [Eq. (85)] is a special case of the general two-manifold Hamiltonian [Eq. (41)]. We shall now introduce a vector notation and define the N component vectors $\mathbf{q}'$ and $\mathbf{q}''$, whose components are q_j' *and* q_j'', $j = 1, \ldots, N$, respectively. The normal modes $\mathbf{q}'$ and $\mathbf{q}''$ are not necessarily the same, and, most generally, they may be related by the transformation

$$\mathbf{q}' = \mathbf{S}\mathbf{q}'' + \mathbf{D}, \tag{88}$$

where $\mathbf{S}$ is the Dushinsky transformation matrix. $\mathbf{D}$ is an N-component vector, whose components D_j denote the dimensionless displacements of the equilibrium positions between the two electronic states. In this section, we shall introduce an additional simplifying assumption, the Condon approximation, which implies that the electronic dipole operator is weakly dependent on the nuclear coordinates, so that μ_{ij} may be simply replaced by the Franck–Condon factors. Setting the electronic dipole matrix element to be unity, we get

$$\mu_{ij} = \langle \mathrm{i}|j\rangle. \tag{89}$$

The molecular eigenstates will be denoted in this section by $|\mathbf{n}\rangle, |\mathbf{m}\rangle, \ldots$, where

$$|\mathbf{n}\rangle = \prod_{j=1}^{N} |n_j\rangle, \tag{90a}$$

$$|\mathbf{m}\rangle = \prod_{j=1}^{N} |m_j\rangle. \tag{90b}$$

In this case, we have:

$$T_{\mathbf{m}''\mathbf{n}''}(\tau) = G_{\mathbf{m}''\mathbf{n}''}(\tau) J_g(\tau), \tag{91a}$$

$$\bar{T}_{\mathbf{m}'\mathbf{n}'}(\tau) = \bar{G}_{\mathbf{m}'\mathbf{n}'}(\tau) J_e(\tau), \tag{91b}$$

$$\hat{T}_{\mathbf{m}'\mathbf{n}'}(\tau) = Z^{-1} \bar{G}_{\mathbf{m}'\mathbf{n}'}(\tau - i\beta) J_g^*(\tau), \tag{91c}$$

where Z is given by Eq. (79d) and the Green's function is defined by

$$G_{\mathbf{m}''\mathbf{n}''}(\tau) = \langle \mathbf{m}'' | \exp(-iH_e\tau) | \mathbf{n}'' \rangle, \tag{92a}$$

$$\bar{G}_{\mathbf{m}'\mathbf{n}'}(\tau) = \langle \mathbf{m}' | \exp(-iH_g\tau) | \mathbf{n}' \rangle. \tag{92b}$$

We shall be interested in calculating the matrix elements of G and $\bar{G}$ [Eq. (92)]. Their calculation is formally very similar, and the expressions for $G_{\mathbf{m}''\mathbf{n}''}(t)$ may be applied to calculate the matrix element $\bar{G}_{\mathbf{m}'\mathbf{n}'}(t)$ by simply changing $\mathbf{D}$ to $-\mathbf{S}^{-1}\mathbf{D}$, $\mathbf{S}$ to $\mathbf{S}^{-1}$, and exchanging ω_j' and ω_j''. It will therefore be sufficient to focus on the evaluation of $G_{\mathbf{m}''\mathbf{n}''}(t)$. By using the generating function of Hermite polynominals and performing a Gaussian integration, it is possible to derive a general expression for $G_{\mathbf{m}''\mathbf{n}''}(\tau)$ for the present model. The final result is considerably simplified when the normal modes in the ground and in the excited electronic states are identical, that is, when the Dushinsky transformation matrix is diagonal

$$S_{ij} = (\omega_i'/\omega_i'')^{1/2} \delta_{ij}. \tag{93}$$

In this case we have (where for brevity we drop the "indexes in $\mathbf{m}''$ and $\mathbf{n}''$),

$$G_{\mathbf{mn}}(t) = \prod_{j=1}^{N} G_{m_j n_j}(t). \tag{94}$$

To simplify the notation, we shall hereafter consider a single mode and omit all the j subscripts from ω_j', ω_j'', D_j, n_j, m_j. The total Green's function can then be calculated using Eq. (94). For a single mode, we have[58]

$$G_{mn}(t) = G_{00}(t) W_{mn}(t) \tag{95}$$

where

$$G_{00}(t) = |\psi(t)|^{-1/2} \exp[D^2 f(t)], \tag{96a}$$

$$\psi(t) = \frac{(\omega_+)^2}{4\omega'\omega''}[1 - (\omega_-/\omega_+)^2 \exp(-2i\omega' t)], \tag{96b}$$

and

$$f(t) = -\frac{\omega''[1 - \exp(-i\omega' t)]}{\omega_+ - \omega_- \exp(-i\omega' t)}. \tag{96c}$$

$W_{mn}(t)$ is given by

$$W_{mn}(t) = (m!n!2^{m+n})^{-1/2} \sum_{p=0}^{m} \sum_{q=0}^{n} (-1)^q \binom{m}{p} \binom{n}{q} [\alpha(t)]^{m+n-p-q} [\tilde{\alpha}(t)]^{p+q} \cdot H_{m+n-p-q}[\lambda f(t) D/\alpha(t)] H_{p+q}(0), \tag{96d}$$

with

$$\omega_\pm = \omega' \pm \omega'', \tag{97a}$$

$$\lambda = (\omega'/\omega'')^{1/2}, \tag{97b}$$

$$\alpha(t) = \left(\frac{1}{2} \frac{\omega_- - \omega_+ \exp(-i\omega' t)}{\omega_+ - \omega_- \exp(-i\omega' t)}\right)^{1/2}, \tag{97c}$$

$$\tilde{\alpha}(t) = \left(\frac{1}{2} \frac{\omega_- + \omega_+ \exp(-i\omega' t)}{\omega_+ + \omega_- \exp(-i\omega' t)}\right)^{1/2}. \tag{97d}$$

Here $H_n(q)$ are the Hermite polynomials. We further have

$$H_n(0) = \begin{cases} 0, & n \text{ odd}, \\ (-1)^{n/2} n!/(n/2)!, & n \text{ even}. \end{cases} \tag{97e}$$

In addition, the ground-state partition function [Eq. (79d)] is given by

$$Z = \prod_{j=1}^{N} [1 - \exp(-\hbar\omega_j''/kT)]^{-1}. \tag{97f}$$

$\tilde{G}_{m'n'}(\tau)$ can be obtained simply by using the substitutions $\omega_j'' \to \omega_j'$, $\omega_j' \to \omega_j''$.

$D_j \rightarrow -(\omega_j''/\omega_j')^{1/2} D_j$ in the expression for $G_{\mathbf{m}'\mathbf{n}'}(\tau)$. The more general expression of $G_{\mathbf{m}'\mathbf{n}'}(\tau)$, which includes the Dushinsky rotation, was derived elsewhere.[58] Equations (91) and (95), together with Eqs. (80)–(84), provide a general, efficient algorithm for calculating any 4WM and SRF lineshape from large polyatomic molecules.

In concluding this section, we present an expression for the absorption lineshape [Eq. (83)]. Using the above definitions, it assumes the form

$$\sigma(\omega) = -2\,\mathrm{Im}\int_0^\infty dt\,\sigma(t) J_g(t)\exp(i\omega t), \tag{98a}$$

where

$$\sigma(t) = \sum_{\mathbf{n}} P(\mathbf{n}) G_{\mathbf{nn}}(t). \tag{98b}$$

The absorption correlation function $\sigma(t)$ at temperature T, is given by[58]

$$\sigma(t) = [\psi_T(t)]^{-1/2} \exp[D^2 f_T(t)], \tag{99a}$$

with

$$\psi_T(t) = \frac{1}{4\omega'\omega''}(\omega'' C_+ A_- + \omega' C_- A_+)(\omega' C_+ A_- + \omega'' C_- A_+) \tag{99b}$$

and

$$f_T(t) = -\frac{\omega'' C_- A_-}{\omega'' C_+ A_- + \omega' C_- A_+}, \tag{99c}$$

where

$$C_\pm = 1 \pm \exp(-i\omega' t), \tag{99d}$$

$$A_\pm = (\bar{n} + 1) \pm \bar{n}\exp(i\omega'' t), \tag{99e}$$

$$\bar{n} = [\exp(\hbar\omega''/kT) - 1]^{-1}. \tag{99f}$$

When $T = 0$ K, $\bar{n} = 0$, and $A_\pm = 1$, we have $\sigma(t) = G_{00}(t)$ [Eq. (96a)]. When $\omega = \omega' = \omega''$, $\psi_T(t) = 1$, $f_T(t) = -\frac{1}{2} C_- A_-$ and Eq. (99a) reduces to,

$$\sigma(t) = \exp\{\tfrac{1}{2}D^2(\bar{n} + 1)[\exp(-i\omega t) - 1] + \tfrac{1}{2}D^2\bar{n}[\exp(i\omega t) - 1]\}. \tag{100}$$

VII. COHERENT VERSUS SPONTANEOUS RAMAN SPECTROSCOPY

There is currently a considerable interest in extracting useful structural and dynamical information on complex molecular systems from spontaneous and coherent Raman lineshapes. Some of the systems extensively studied are conjugated polyenes, aromatic molecules, and molecules of biological interest, such as porphyrins and β-carotenes in solution.[7-12,34-56] Raman lines are narrow, two-photon resonances, which occur both in spontaneous emission and in 4WM (coherent Raman) spectroscopy. In this section, we make a specific application of our general results to Raman lineshapes. We shall first present the expressions for these two types of Raman experiments and then compare them in detail. We start with spontaneous Raman spectroscopy. Typically, it is possible to distinguish between two types of contributions to the spontaneous emission spectra of polyatomic molecules in condensed phases. These are denoted as Raman and fluorescence, respectively.[11,69-75] The fluorescence component is sometimes referred to as hot luminescence or redistribution. The Raman components are relatively narrow emission lines occurring at $\omega_1 - \omega_2 = \omega_{ca}$, where $|a\rangle$ and $|c\rangle$ are any pair of ground-state vibronic levels, and their widths are narrower than a few cm^{-1}. The fluorescence lines in solution are much broader (typical width of a few hundred cm^{-1}), and their maxima occur at $\omega_2 = \omega_{bc}$, where levels $|b\rangle$ and $|c\rangle$ belong to the excited and the ground electronic states, respectively (Fig. 2). A clear distinction between these two components may be made by tuning ω_1 across the absorption spectrum. The Raman lines, which occur at a fixed $\omega_1 - \omega_2$, will follow the tuning of ω_1, whereas the fluorescence components will remain roughly in the same positions. The origin of these components can be understood by a close examination of Eq. (84). Consider the third term [pathway (iii)] in Eq. (84). Let us further assume that $\Gamma_{ca} = 0$, which implies an infinite lifetime for vibronic states belonging to the ground electronic state. We then have

$$\frac{1}{\omega_2 - \omega_1 + \omega_{ca}} = -i\pi\delta(\omega_2 - \omega_1 + \omega_{ca}) + \mathrm{PP}\left(\frac{1}{\omega_2 - \omega_1 + \omega_{ca}}\right), \quad (101)$$

where PP stands for the principal part. The $\delta(\omega_2 - \omega_1 + \omega_{ca})$ term will contribute to the Raman component, whereas all the rest of the terms in Eq. (84) will not contain any such resonance and will constitute the "fluorescence." We thus have[64]

$$S_{\mathrm{SRF}}(\omega_1, \omega_2) = S_{\mathrm{RAMAN}}(\omega_1, \omega_2) + S_{\mathrm{FL}}(\omega_1, \omega_2), \quad (102a)$$

$$S_{\mathrm{RAMAN}}(\omega_1, \omega_2) = 2\pi \sum_{a,c} P(a)|K_{ca}(\varepsilon_a + \omega_1)|^2 \delta(\omega_2 - \omega_1 + \omega_{ca}), \quad (102b)$$

and

$$S_{FL}(\omega_1,\omega_2) = 2\,\mathrm{Im}\left[\sum_{b,d}\frac{[\bar{K}_{bd}(\varepsilon_b-\omega_2)-\bar{K}^*_{db}(\varepsilon_d-\omega_2)]\bar{K}_{db}(\varepsilon_b-\omega_1)}{\omega_{bd}+i\Gamma_{bd}}\right.$$
$$\left.+\,\mathrm{PP}\left(\sum_{a,c}P(a)\frac{K_{ca}(\varepsilon_c+\omega_2)K^*_{ca}(\varepsilon_a+\omega_1)}{\omega_2-\omega_1-\omega_{ca}}\right)\right]. \tag{102c}$$

For isolated molecules, in the absence of a bath, an interesting destructive interference takes place, whereby all the contributions to the fluorescence cancel exactly. We then have $S_{FL}=0$, and the total emission is of the Raman type. Equations (102) then reduce to the Kramer–Heisenberg formula,[76] which can be derived using second-order perturbation theory. The situation is more complicated, however, for spontaneous emission spectra in condensed phases (solutions, matrices, molecular crystals, glasses, chromophores on proteins, etc.). In these cases, the molecule is subject to a random force, resulting from its interaction with a macroscopic number of external degrees of freedom, which constitute a thermal bath. The random force results in a significant line broadening and a loss of much of the structure in these spectra. It also "redistributes" the emitted intensity by reducing the Raman and building the fluorescence component instead. There are three types of experimental observables in a molecular Raman experiment: (1) the absorption spectrum, $\sigma(\omega_1)$ [Eq. (83)]; (2) the excitation profiles $|K_{ca}(\varepsilon_a+\omega_1)|^2$ [Eq. (102b)], obtained by tuning ω_1 and detecting the narrow Raman component at $\omega_2-\omega_1=\omega_{ac}$ each pair of ground vibronic states $|a\rangle$ and $|c\rangle$ has its distinct excitation profile; and (3) the fluorescence spectrum, $S_{FL}(\omega_1,\omega_2)$ [Eq. (102c)]. These will be discussed following the introduction of coherent Raman lineshapes.

We shall now consider coherent Raman measurements (CARS and CSRS),[3,4,14,34–43] which are the coherent analogue of the spontaneous Raman spectra. Coherent Raman experiments are a special type of 4WM. They involve two incoming fields (i.e., $\mathbf{k}_3=\mathbf{k}_1$), and the signal mode is

$$\mathbf{k}_s = 2\mathbf{k}_1-\mathbf{k}_2, \tag{103a}$$
$$\omega_s = 2\omega_1-\omega_2. \tag{103b}$$

Since two fields are identical, there are only three permutations of the frequencies (and not six). Writing the frequency permutations explicitly, we get

$$\chi^{(3)}(-\omega_s,\omega_1,-\omega_2,\omega_1) = \hat{R}(2\omega_1-\omega_2,\omega_1-\omega_2,\omega_1)$$
$$+\,\hat{R}(2\omega_1-\omega_2,\omega_1-\omega_2,-\omega_2)$$
$$+\,\hat{R}(2\omega_1-\omega_2,2\omega_1,\omega_1), \tag{104}$$

where $\hat{R}$ is given in Eq. (63). $\chi^{(3)}$ thus contains $3 \times 8 = 24$ terms. In coherent Raman spectroscopy we look for two-photon resonances in the signal, which occur when $\omega_1 - \omega_2$ equals an energy difference between two ground-state or excited-state vibrational states. For our level scheme (Fig. 4) such resonances occur for $\omega_1 - \omega_2 = \pm\omega_{ca}$ or for $\omega_1 - \omega_2 = \pm\omega_{db}$. The names CARS and CSRS refer to the cases where $\omega_1 > \omega_2$ or $\omega_1 < \omega_2$, respectively. Since there are no fundamental differences between the theoretical treatments of the two, we shall focus on the CARS resonances,

$$\omega_1 - \omega_2 = \omega_{ca} \tag{105a}$$

and

$$\omega_1 - \omega_2 = \omega_{db}. \tag{105b}$$

Equation (105a) represents ground-state CARS and Eq. (105b) represents excited-state CARS. It is clear that the third term in Eq. (104), $\hat{R}(2\omega_1 - \omega_2, 2\omega_1, \omega_1)$, cannot contribute to CARS since its two-photon frequency is $2\omega_1$ and not $\omega_1 - \omega_2$. We shall therefore ignore this term. Let us denote the eight pathways of the first term in Eq. (104) by (i)–(viii), and the corresponding ones for the second term in Eq. (104) by (i)′–(viii)′. (See Fig. 6.) Starting with ground-state CARS, we note that there are eight terms containing an $\omega_1 - \omega_2 \pm \omega_{ca}$ denominator. These correspond to diagrams (i), (iv), (v), (viii), and (i)′, (iv)′, (v)′, and (viii)′, that is,

$$\chi^{(3)}_{ca} = \sum_{b,d} \mu_{ab}\mu_{bc}\mu_{cd}\mu_{da}[I_{ba}(2\omega_1 - \omega_2) + I^*_{bc}(\omega_2 - 2\omega_1)] \times \frac{P(a)I_{da}(\omega_1) + P(a)I_{da}(-\omega_2) - P(c)I^*_{dc}(-\omega_1) - P(c)I^*_{dc}(\omega_2)}{\omega_1 - \omega_2 - \omega_{ca} + i\Gamma_{ac}} \tag{106a}$$

where the subscript ca denotes that these are ground-state ($\omega_1 - \omega_2 = \omega_{ca}$) resonances. In the terms corresponding to pathways (i), (i)′, (iv), (iv)′, we have interchanged the dummy summation indexes a and c, and b and d, in order to recast these expressions into a more compact form. We shall now invoke the rotating wave approximation (RWA), in which we retain only resonant terms in which all denominators contain a difference of a field frequency and a molecular optical frequency, and neglect all terms where at least one denominator is antiresonant. For the ground-state CARS, the only surviving terms are (iv)′ and (v), that is,

$$\chi^{(3)}_{ca} = \sum_{b,d} \mu_{ab}\mu_{bc}\mu_{cd}\mu_{da} \frac{I_{ba}(2\omega_1 - \omega_2)[P(a)I_{da}(\omega_1) - P(c)I^*_{dc}(\omega_2)]}{\omega_1 - \omega_2 - \omega_{ca} + i\Gamma_{ac}}. \tag{106b}$$

In addition, there are eight terms in Eq. (104), which contain an $\omega_1 - \omega_2 - \omega_{db}$ denominator. These correspond to pathways (ii), (iii), (vi), (vii) and (ii)', (iii)', (vi)', and (vii)', that is,

$$\chi^{(3)}_{db} = \sum_{a,c} P(a)\mu_{ab}\mu_{bc}\mu_{cd}\mu_{da}[\bar{I}_{dc}(2\omega_1 - \omega_2) + \bar{I}^*_{bc}(\omega_2 - 2\omega_1)] \times \frac{I_{da}(\omega_1) + I_{da}(-\omega_2) - I^*_{ba}(-\omega_1) - I^*_{ba}(\omega_2)}{\omega_1 - \omega_2 - \omega_{db} + i\Gamma_{db}} \tag{107a}$$

Within the RWA, only two terms contribute to $\chi^{(3)}_{db}$, which come from pathways (ii) and (iii)', that is,

$$\chi^{(3)}_{db} = \sum_{a,c} P(a)\mu_{ab}\mu_{bc}\mu_{cd}\mu_{da}\frac{\bar{I}_{dc}(2\omega_1 - \omega_2)[I_{da}(\omega_1) - I^*_{ba}(\omega_2)]}{\omega_1 - \omega_2 - \omega_{db} + i\Gamma_{db}}. \tag{107b}$$

Making use of Eqs. (106b) and (107b), we have finally

$$\begin{aligned}\chi^{(3)}_{\mathrm{CARS}} &= \sum_{a,c}\chi^{(3)}_{ac} + \sum_{b,d}\chi^{(3)}_{db} \\ &= \sum_{a,b,c,d} P(a)\mu_{ab}\mu_{bc}\mu_{cd}\mu_{da} \\ &\quad\times\left(\frac{I_{ba}(2\omega_1 - \omega_2)[I_{da}(\omega_1) - \exp(-\omega_{ca}/kT)I^*_{dc}(\omega_2)]}{\omega_1 - \omega_2 - \omega_{ca} + i\Gamma_{ca}}\right. \\ &\quad\left.+\frac{\bar{I}_{dc}(2\omega_1 - \omega_2)[I_{da}(\omega_1) - I^*_{ba}(\omega_2)]}{\omega_1 - \omega_2 - \omega_{db} + i\Gamma_{db}}\right).\end{aligned} \tag{108}$$

Making use of Eqs. (81), we may recast the CARS signal generated at $\mathbf{k}_s = 2\mathbf{k}_1 - \mathbf{k}_2$ into the form

$$S_{\mathrm{CARS}}(\omega_1, \omega_2) = |\chi^{(3)}_{\mathrm{CARS}}(-\omega_s, \omega_1, -\omega_2, \omega_1)|^2, \tag{109a}$$

where

$$\begin{aligned}&\chi^{(3)}_{\mathrm{CARS}}(-\omega_s, \omega_1, -\omega_2, \omega_1) \\ &= \sum_{a,c}\frac{P(a)K_{ac}(\varepsilon_a + 2\omega_1 - \omega_2)[K_{ca}(\varepsilon_a + \omega_1) - \exp(-\omega_{ca}/kT)K^*_{ac}(\varepsilon_c + \omega_2)]}{\omega_1 - \omega_2 - \omega_{ca} + i\Gamma_{ca}} \\ &\quad+\sum_{b,d}\frac{\bar{K}^*_{db}(\varepsilon_d - 2\omega_1 + \omega_2)[\bar{K}^*_{bd}(\varepsilon_d - \omega_1) - \bar{K}_{db}(\varepsilon_b - \omega_2)]}{\omega_1 - \omega_2 - \omega_{db} + i\Gamma_{db}}.\end{aligned} \tag{109b}$$

For comparison, the spontaneous Raman signal [Eq. (102b)] is given by

$$S_{\text{RAMAN}}(\omega_1,\omega_2) = -2\,\text{Im}\,\chi^{(3)}_{\text{RAMAN}}(-\omega_2,\omega_2,-\omega_1,\omega_1), \tag{110a}$$

where

$$\chi^{(3)}_{\text{RAMAN}}(-\omega_2,\omega_2,-\omega_1,\omega_1) \equiv \sum_{a,c} P(a)\frac{K_{ca}(\varepsilon_c+\omega_2)K^*_{ca}(\varepsilon_a+\omega_1)}{\omega_2-\omega_1+\omega_{ca}+i\Gamma_{ca}}. \tag{110b}$$

For molecules in solution, Γ_{ac} and Γ_{bd} are usually much smaller than a characteristic line broadening, which is typically a few hundred cm^{-1}. A Lorentzian with a width of Γ_{ac} or Γ_{bd} may therefore be approximated by a delta function. We then write

$$\left|\frac{1}{\omega_1-\omega_2-\omega_{ca}+i\Gamma_{ca}}\right|^2 \cong \frac{\pi\delta(\omega_1-\omega_2-\omega_{ca})}{\Gamma_{ca}}, \tag{111a}$$

$$\left|\frac{1}{\omega_1-\omega_2-\omega_{db}+i\Gamma_{db}}\right|^2 \cong \frac{\pi\delta(\omega_1-\omega_2-\omega_{db})}{\Gamma_{db}}, \tag{111b}$$

and

$$\text{Im}\frac{1}{\omega_2-\omega_1+\omega_{ca}} = -\pi\delta(\omega_2-\omega_1+\omega_{ca}). \tag{111c}$$

Making use of Eqs. (109)–(111) and ignoring background terms, we get finally

$$S_{\text{CARS}} = \sum_{a,c} Q^g_{ac}(\omega_1)\delta(\omega_1-\omega_2-\omega_{ca}) + \sum_{b,d} Q^e_{bd}(\omega_1)\delta(\omega_1-\omega_2-\omega_{db}) \tag{112a}$$

and

$$S_{\text{RAMAN}} = \sum_{a,c} Q_{ac}(\omega_1)\delta(\omega_1-\omega_2-\omega_{ca}), \tag{112b}$$

where

$$Q^g_{ac}(\omega_1) = \frac{\pi}{\Gamma_{ca}}|P(a)K_{ac}(\varepsilon_c+\omega_1)|^2|K_{ca}(\varepsilon_a+\omega_1) - \exp(-\omega_{ca}/kT)K^*_{ac}(\varepsilon_a+\omega_1)|^2, \tag{112c}$$

$$Q^e_{bd}(\omega_1) = \frac{\pi}{\Gamma_{db}}|\bar{K}_{db}(\varepsilon_b-\omega_1)|^2|\bar{K}^*_{bd}(\varepsilon_d-\omega_1) - \bar{K}_{db}(\varepsilon_d-\omega_1)|^2, \tag{112d}$$

$$Q_{ac}(\omega_1) = 2\pi P(a)|K_{ca}(\varepsilon_a+\omega_1)|^2. \tag{112e}$$

$Q^g_{ac}(\omega_1)$ is the coherent Raman excitation profile corresponding to a ground-state resonance, and $Q^e_{bd}(\omega_1)$ is the coherent Raman excitation profile for an excited-state resonance. $Q_{ac}(\omega_1)$ is the spontaneous Raman excitation profile. These profiles are easily measured by probing the intensity of a particular Raman line ($\omega_1 - \omega_2$ fixed) as a function of ω_1. It should be noted that the excited-state resonances Q^e_{db} are induced by the interaction with the bath. In the absence of a bath, an interference causes these resonances to vanish.[6,16,17,21] The excited-state cars resonances are therefore induced by dephasing.

The present formulation provides rigorous microscopic relations of 4WM and SRF lineshapes to standard correlation functions of the medium that can be evaluated by a variety of methods. Such methods include density expansions for pressure broadening in the gas phase and in liquids,[11,77-80] cumulant expansions for phonon broadening,[81,82] and semiclassical and molecular dynamics simulations.[83-86] For polar solvents, it is possible to use a continuum dielectric model for the solvent and relate the necessary correlation functions to the frequency-dependent dielectric constant $\varepsilon(\omega)$.[68,87-92] For the sake of illustration, we now present some calculations performed using a simplified stochastic model, whereby the effect of the bath is modeled as a stochastic Gaussian modulation of the electronic energy gap.[93-95] We assume that due to the random force exerted on the molecule by the bath, the electronic energy gap ω_{eg} becomes a stochastic function of time (Figs. 2 and 9) and the Hamiltonian [Eq. (85)] assumes the form[44,45,64]

$$H = |g\rangle H_g(Q_s)\langle g| + |e\rangle[\omega_{eg} + \delta\omega_{eg}(t) + H_e(Q_s) - i\gamma/2]\langle e|, \quad (113a)$$

where $\delta\omega_{eg}(t)$ is assumed to be a Gaussian Markov process with

$$\langle \delta\omega_{eg}(t)\rangle = 0, \quad (113b)$$

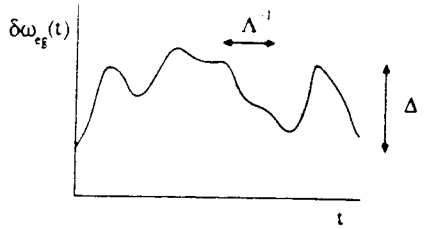

Figure 9. The stochastic process $\delta\omega_{eg}(t)$ representing the time-dependent molecular electronic energy gap in a solution [Eq. (113)]. Δ represents the magnitude of the fluctuations, and Λ^{-1} represents their time scale.

and

$$\langle \delta\omega_{eg}(t)\delta\omega_{eg}(0)\rangle = \Delta^2 \exp(-\Lambda t). \tag{113c}$$

Here, the angular brackets $\langle \cdots \rangle$ denote averaging over the stochastic process, Δ is the root-mean-squared amplitude of the fluctuations, and Λ^{-1} is the correlation time of the bath fluctuations. Equations (113) can be obtained from our microscopic model [Eq. (41)] by taking the bath degrees of freedom to be classical and assuming that the bath is sufficiently large that its motions are independent of the absorber. By going to the interaction picture (with respect to the bath Hamiltonian), we may then recast Eq. (41) in the form of Eqs. (113). Within this model, the bath is affecting the system, but the system is not affecting the bath. The Gaussian nature of $\delta\omega_{eg}(t)$ may usually be justified using the central limit theorem. This choice of a stochastic Hamiltonian is based on the assumption that the bath couples mainly to the electronic degrees of freedom, so that the ground-state and the excited-state vibronic manifolds are being stochastically modulated with respect to each other, but no modulation occurs for frequencies of levels belonging to the same electronic manifold, that is, vibrational dephasing is neglected. This is often a realistic assumption. The nonlinear response function can be evaluated also for a more general class of stochastic models.[19] However, for the sake of simplicity we shall restrict the present discussion to this special case. For this model, we have[93-95]

$$J_e(t) = J_g(t) = \exp\{-(\Delta/\Lambda)^2[\exp(-\Lambda t) - 1 + \Lambda t]\}. \tag{114}$$

This simple model provides a good insight on the effect of the bath. Generalization to more complicated situations, whereby $J_e(t) \neq J_g(t)$, and relating Δ and Λ to more microscopic properties of the solvent can be made without a major difficulty.[68] The nature of the lineshape function [Eqs. (64)] depends on the dimensionless parameter

$$\kappa = \Lambda/\Delta. \tag{115}$$

The *fast modulation* (homogeneous) limit is obtained when the correlation time of the bath fluctuations is very fast compared with their magnitude, that is, $\kappa \gg 1$. In this case, the $\exp(-\Lambda\tau)$ on the right-hand side of Eq. (114) vanishes very rapidly and may be ignored. We then get

$$J_e(t) = J_g(t) = \exp(-\hat{\Gamma} t), \tag{116a}$$

where

$$\hat{\Gamma} = \Delta^2/\Lambda. \tag{116b}$$

The absorption lineshape function [Eq. (64)] assumes a Lorentzian form corresponding to homogeneous dephasing, that is,

$$I_{\nu\lambda}(\omega) = \frac{1}{\omega - \omega_{\nu\lambda} + i\Gamma}, \tag{116c}$$

where $\Gamma = \hat{\Gamma} + \gamma/2$. The *slow modulation* (static, inhomogeneous) limit is obtained when $\Lambda \ll \Delta$, that is, $\kappa \ll 1$. In this case, we can make a Taylor expansion of Eq. (114) (short-time approximation) resulting in

$$J_e(t) = J_g(t) = \exp[-\Delta^2 t^2/2]. \tag{116d}$$

The absorption lineshape [the imaginary part of Eq. (64)] assumes, in this case, the Voigt profile (a convolution of a Gaussian and a Lorentzian), and, when $\gamma \ll \Delta$, it becomes a Gaussian. As κ is increased, the absorption lineshape thus changes continuously from a Gaussian to a Lorentzian. The full width at half maximum Γ_0 of the absorption lineshape [the imaginary part of $I_{\nu\lambda}(\omega)$] is displayed in Fig. 10 versus κ and may be adequately approximated by the Padé approximant[44]

$$\frac{\Gamma_0}{\Delta} = \frac{2.355 + 1.76\kappa}{1 + 0.85\kappa + 0.88\kappa^2}. \tag{117}$$

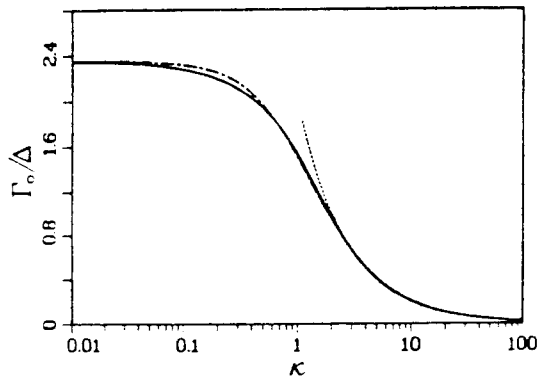

Figure 10. The full width at half maximum (Γ_0/Δ) of the stochastic lineshape function $\sigma(\omega)$ for a two-level system versus κ [Eqs (98a) and (114) with $\sigma(t) = 1$)], $\gamma = 0$. Solid line is the exact curve (calculated numerically); dot-dashed line is the Padé approximant, Eq. (117); short dashed line is $\Gamma_0/\Delta = 2\kappa$, which holds in the fast modulation limit when $\kappa \gg 1$ [Eq. (116a)].

The model Hamiltonian defined by Eqs. (85) and (113) is exactly solvable, and we have derived explicit closed-form expressions for the nonlinear response function [Eq. (49)] and for the SRF lineshape [Eq. (75)].[44,45,64] The exact result is in the form of an infinite series, whose first term corresponds to the factorization approximation [Eqs. (82) and (84)]. The factorization approximation was shown to be exact in the fast modulation limit, $\kappa \gg 1$. In addition, under quite general conditions ($\Lambda \gg \gamma$), the "rapid fluctuation" limit, the factorization approximation holds for an arbitrary value of κ and provides an excellent approximation over a wide range of broadening parameters. We shall now present numerical calculations of coherent and spontaneous Raman spectroscopy using Eqs. (112) and (113).[45] We first consider a diatomic molecule, with a single vibrational mode, $\omega'' = 1000\ \text{cm}^{-1}$, $\omega' = 875\ \text{cm}^{-1}$, and the dimensionless displacement $D = 1.5$. The temperature is assumed to be low compared with ω'' ($\hbar\omega'' \ll kT$), so that at equilibrium the molecule is in the ground vibronic state. We have calculated the absorption lineshape [Eq. (98)], the dispersed fluorescence $S_{\text{SRF}}(\omega_1, \omega_2)$ [Eq. (102)], and the CARS signal $S_{\text{CARS}}(\omega_1, \omega_2)$ [Eq. (109)]. $K(\omega)$, $\bar{K}(\omega)$, and $\tilde{K}(\omega)$ were calculated using Eqs. (81) and a standard fast Fourier routine. We used 8192 points of integration with a time step of $\Delta t = 10^{-15}$ sec. In Fig. 11 we display the absorption $\sigma(\omega)$, the dispersed fluorescence $S_{\text{SRF}}(\omega_1, \omega_2)$ and the CARS signal $S_{\text{CARS}}(\omega_1, \omega_2)$ for our model. $S_{\text{SRF}}(\omega_1, \omega_2)$ and $S_{\text{CARS}}(\omega_1, \omega_2)$ are displayed as a function of ω_2, with ω_1 fixed at the origin 0–0 transition frequency. The absorption spectrum shows a progression of the excited-state frequency ($\omega' = 1000\ \text{cm}^{-1}$). The dispersed fluorescence consists of a series of broad bands ("fluorescence") and narrow lines ("Raman"), which are peaked at $\omega_1 - \omega_2 = n\omega''$. Similarly, the CARS signal S_{CARS} contains a series of ground-state narrow resonances at $\omega_1 - \omega_2 = n\omega''$ and a series of excited-state narrow resonances peaked at $\omega_1 - \omega_2 = n\omega'$. S_{CARS} thus reveals both the ground-state and the excited-state frequencies and is more informative than S_{SRF}.[16,17,21] We shall now consider the Raman excitation profiles for our model $Q^g_{ac}(\omega_1)$, $Q^e_{bd}(\omega_1)$, and $Q_{ac}(\omega_1)$. In Fig. 12, we compare the spontaneous and the coherent Raman excitation profiles of β carotene, calculated by using a harmonic model with three Raman active modes. Eqs. (112) were modified to take the degeneracy in ω_{ac} and ω_{bd} into account. The broadening parameters were obtained by a fit to experimental spontaneous Raman profiles, and the coherent Raman profiles are predictions using our theory. The details of the calculations are presented in Ref. 96. We have further used the present stochastic model for harmonic molecules to calculate the absorption and the Raman excitation profiles of the 700 nm ($S_0 - S_1$) transition of azulene.[44] The available experimental data[46] consist of the absorption; the Raman fundamentals of the 1400, 1200, and the 900 cm^{-1} modes; and the first Raman overtone of the 825 cm^{-1} mode. The measurements were made at room

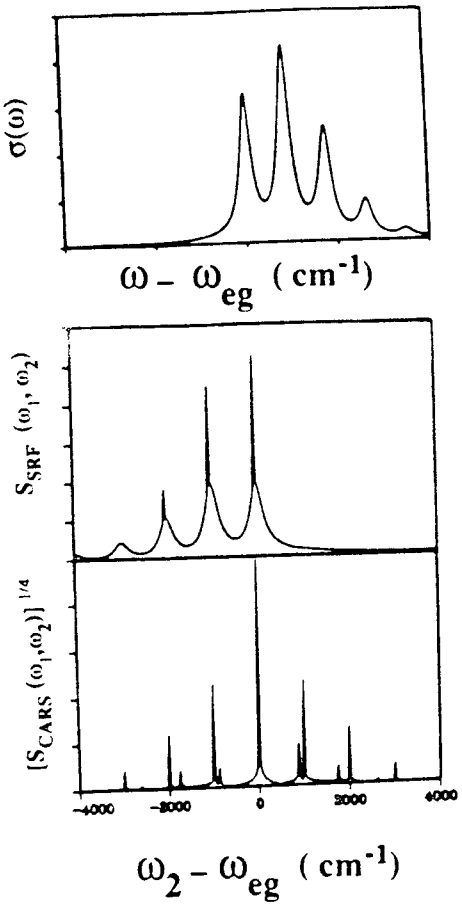

Figure 11. Absorption, SRF, and coherent Raman emission for a diatomic molecule with a single vibrational mode $\omega'' = 1000\ \text{cm}^{-1}$, $\omega' = 875\ \text{cm}^{-1}$, and the dimensionless displacement $D = 1.5$. The calculation was done in the fast modulation limit [Eq. (116a)] with $\Gamma = 1000\ \text{cm}^{-1}$ and $\gamma = 0$. The absorption spectrum $\sigma(\omega)$ was calculated using Eq. (98a). The SRF spectrum $S_{\text{SRF}}(\omega_1, \omega_2)$ [Eq. (102)] and the coherent Raman signal $S_{\text{CARS}}(\omega_1, \omega_2)$ [Eq. (109)] are plotted versus ω_2. For clarity we have plotted the fourth root of the coherent Raman signal $[S_{\text{CARS}}(\omega_1, \omega_2)]^{1/4}$. ω_1 was taken to be on resonance with the fundamental (0–0) transition, $\omega_1 = \omega_{eg}$.[45]

temperature using CS_2 as a solvent. All calculations were made using Eqs. (112). $G_{mn}(t)$ were first calculated using Eq. (95), and $K_{mn}(\omega)$ [Eqs. (81)] were then computed using a standard fast Fourier transform routine. We used 8192 time points with a step size of $\Delta t = 6.4 \times 10^{-15}$ sec. The ground-state and the excited-state seven-mode frequencies ω' and ω'' were taken from Ref. 46, and the displacements D_j and the broadening parameters (Δ and Λ) were adjusted

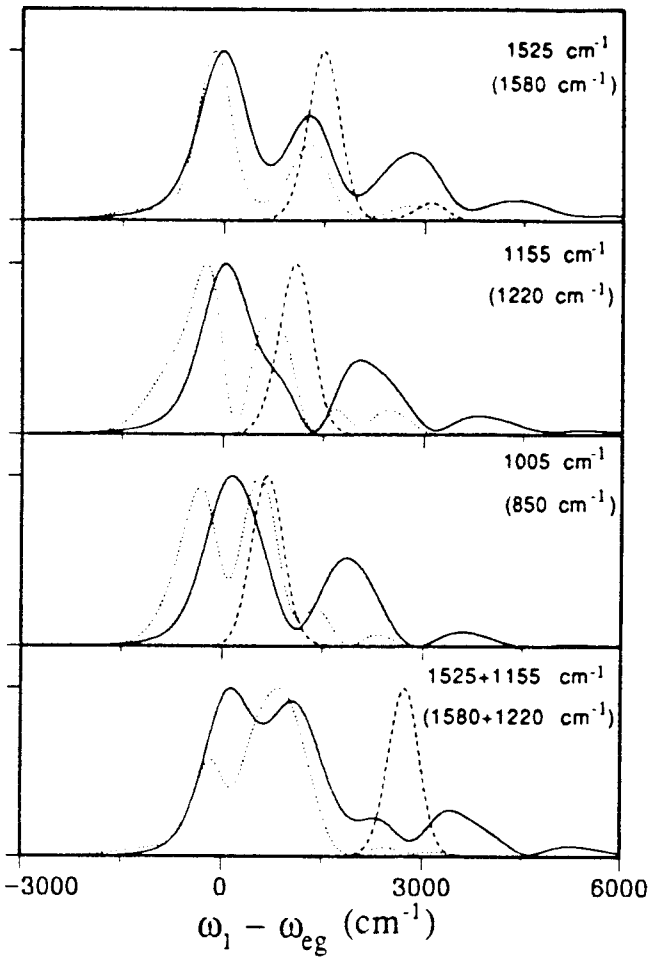

Figure 12. Calculated Raman excitation profiles of β carotene. A harmonic three-mode model was used with ground state frequencies $\omega_1'' = 1525$, $\omega_2'' = 1155$, and $\omega_3'' = 1005\ \text{cm}^{-1}$ and excited state frequencies $\omega_1' = 1580$, $\omega_2' = 1220$, and $\omega_3' = 850\ \text{cm}^{-1}$. The displacements are $D_1 = 1.12$, $D_2 = .95$, and $D_3 = .65$. The broadening parameters are $\Delta = 362\ \text{cm}^{-1}$ and $\Lambda = 109\ \text{cm}^{-1}$ corresponding to $\kappa = 0.3$ and $\Gamma_0 = 760\ \text{cm}^{-1}$. In each panel we show the spontaneous Raman $Q_{ac}(\omega_1)$ (solid line), the Raman excitation profile corresponding to ground-state resonance $Q_{ac}^{g}(\omega_1)$ (dotted line), and the corresponding excited-state resonance $Q_{bd}^{e}(\omega_1)$ (dashed line). The Raman frequency ω_{ca} is indicated in each panel; the corresponding excited-state frequency ω_{db} is indicated in parentheses.[96]

TABLE I
Ground-State and Excited-State Frequencies and the Dimensionless Displacements Used in our Best-Fit Seven-Mode Calculation of Azulene[44-46]

Mode	ω_j'' (cm^{-1})	ω_j' (cm^{-1})	D_j
1	406	384	0.61
2	679	662	0.76
3	825	857	1.23
4	900	900	0.55
5	1260	1193	0.77
6	1400	1388	1.09
7	1562	1550	1.12

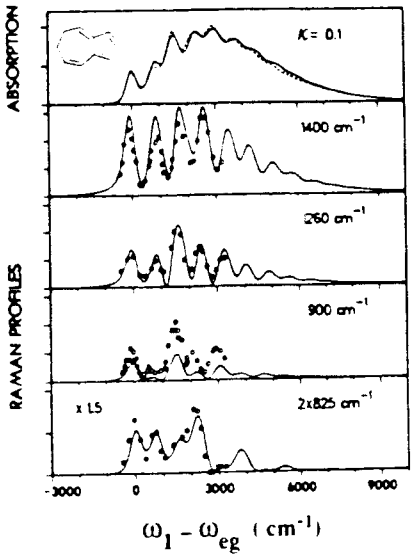

Figure 13. Absorption and resonance Raman profiles for azulene in CS_2 at 300 K.[44] The solid lines are theoretical curves computed using a seven-mode stochastic harmonic model without Dushinsky rotation (Table I). The absorption curve (upper panel) is $\omega\sigma(\omega)$, where $\sigma(\omega)$ is given in Eq. (98a). The dashed line represents the experimental data.[46] The Raman profiles (lower four panels) were calculated using Eq. (112e). Shown are the experimental data[46] (circles) and the calculated profiles $Q_{ac}(\omega_1)$ for four different Raman transitions, as indicated in each panel. The broadening parameters are $\Delta = 180$ cm^{-1}, $\Lambda = 18$ cm^{-1}, and $\Gamma_0 = 408$ cm^{-1}, $\gamma = 0$ and $\omega_{eg} = 14{,}286$ cm^{-1}.

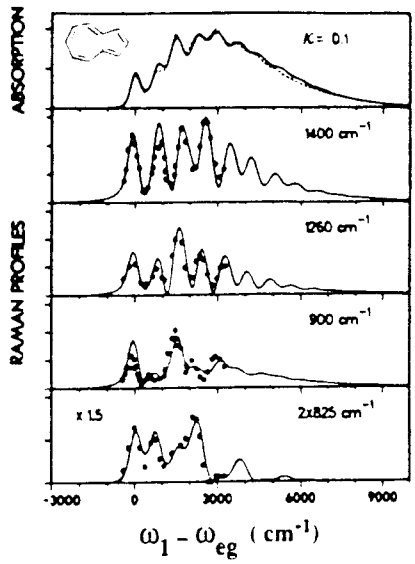

Figure 14. The same as Fig. 13, but with a Dushinsky rotation included. We have used a 2 × 2 Dushinsky rotation matrix, coupling the 900 cm^{-1} and the 1400 cm^{-1} modes. The off-diagonal element $S_{4,6}$ between these modes is -0.20 [Eq. (88)].

to fit the data. We first attempted to obtain the best fit without a Dushinsky rotation, making use of Eqs. (93)–(95) for $G_{mn}(t)$. The structural parameters of our best fit are given in Table I. The solvent line-broadening parameters of our fit are $\Delta = 180$ cm^{-1}, $\Lambda = 18$ cm^{-1} corresponding to $\kappa = 0.1$, and $\Gamma_0 = 408$ cm^{-1} (Fig. 10). The resulting lineshapes are shown in Fig. 13. It is clear that the overall fit for the absorption and the 1400, 1260, and 825 cm^{-1} modes is satisfactory. The calculated intensity of the 900 cm^{-1} vibration (mode 4) is too weak, and that of the 1400 cm^{-1} vibration (mode 6) is too strong. We therefore introduced a Dushinsky rotation parameter to couple the 1400 and 900 cm^{-1} modes, keeping all other parameters fixed, and we were then able to obtain a good simultaneous fit of the absorption and all the Raman profiles.[44,58] The resulting Dushinsky rotation parameter ($S_{4,6} = -0.20$) is the same as that obtained in Ref. 46. Our best fit is displayed in Fig. 14. In Figs. 15 and 16 we demonstrate the dependence of our lineshapes on κ. In these figures we kept the same structural parameters of Fig. 14 and varied κ ($\kappa = 1, \infty$) keeping the full width at half maximum of the absorption lineshape Γ_0 [Eq. (117)] fixed. The absorption lineshape for these new parameters is virtually identical to that obtained from the parameters of Figs. 13 and 14. The excitation profiles, however, are significantly different. These calculations demonstrate the advantages of the present theory. As the number of modes

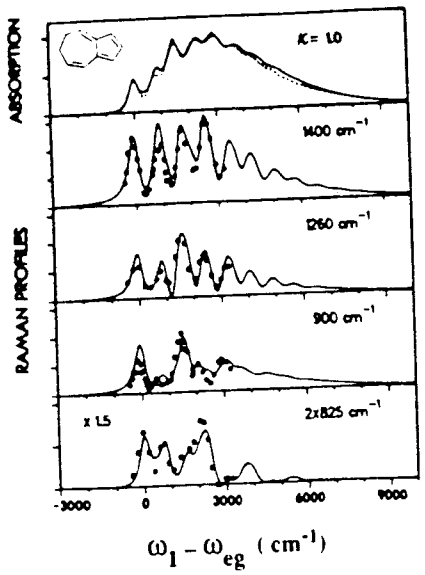

Figure 15. The same as Fig. 14 with different broadening parameters, $\Delta = 266\ cm^{-1}$, $\Lambda = 266\ cm^{-1}$ corresponding to $\kappa = 1$ and with the same value of Γ_0, that is, $\Gamma_0 = 408\ cm^{-1}$.[44]

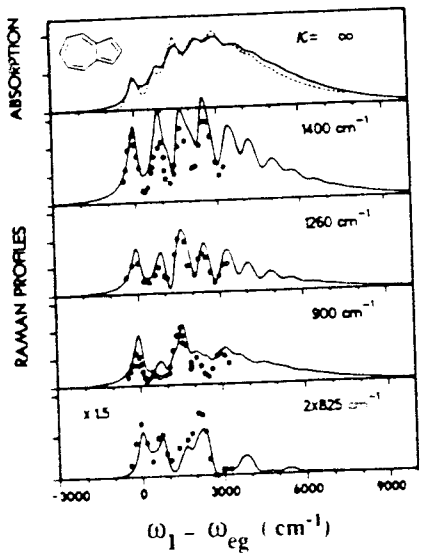

Figure 16. The same as Fig. 14 with different broadening parameters corresponding to the fast modulation limit, $\kappa = \infty$, with the same value of Γ_0, that is, $\Gamma_0 = 2\Delta^2/\Lambda = 408\ cm^{-1}$.[44]

increases, the conventional expressions, based on summations over eigenstates, become intractable. The computational effort involved in the present Fourier transform method does not increase substantially as the molecular size increases, since a single Fourier transform is required in any case.

VIII. THE ROLE OF VIBRATIONAL RELAXATION IN SPONTANEOUS RAMAN AND FLUORESCENCE SPECTROSCOPY

So far we considered only dephasing effects of the thermal bath, that is, the interaction between the system and the bath was taken to be diagonal in the system states [Eq. (41)]. This interaction results in line broadening and also induces new components in the spectra (e.g., the fluorescence and the excited-state resonances in CARS). An important process, which takes place in polyatomic molecules in solution, is vibrational relaxation (VR).[59] The vibrational state of the system following the optical transition is determined by the incident light frequency and by the Franck–Condon factors, and it is usually a nonequilibrium state. The interactions with the solvent will result in vibrational relaxation, which will tend to equilibrate the optically excited molecule with the bath temperature. A microscopic treatment of these processes requires introducing a specific model for the interaction between the system and the bath into the Hamiltonian, Eq. (41). However, it is convenient and often satisfactory to treat these processes phenomenologically via the Pauli master equation.[97] This is done by adding a relaxation matrix to the Liouville equation. The procedure is similar for 4WM and for SRF lineshapes. In this section we shall focus explicitly on SRF. The extension to 4WM is straightforward. The phenomenological VR matrix is introduced by modifying the Liouville operator [Eq. (9a)]. We define

$$L\rho = [H, \rho] - i\Gamma\rho, \tag{118}$$

where H is the molecular Hamiltonian [Eq. (41)] and Γ is the relaxation matrix, which includes vibrational and radiative relaxation. For simplicity we consider only VR within the electronically excited state. Including ground-state VR can be made in a similar way. The Liouville space operator Γ is defined by its matrix elements, that is,

$$\langle\langle b'b'|\Gamma|bb\rangle\rangle \equiv -\gamma_{b'b}, \qquad b' \neq b, \tag{119a}$$

$$\langle\langle bb|\Gamma|bb\rangle\rangle = \sum_{b' \neq b} \gamma_{b'b} + \gamma_r \equiv \gamma_b. \tag{119b}$$

Γ further satisfies the detailed balance condition

$$\gamma_{b'b} = \gamma_{bb'} \exp(-\omega_{b'b}/kT). \tag{119c}$$

In addition, we have the decay rate of coherences

$$\langle\langle bb'|\Gamma|bb'\rangle\rangle = -\tfrac{1}{2}(\gamma_b + \gamma_{b'}) \equiv \Gamma_{bb'}. \tag{119d}$$

Here, $\gamma_{b'b}$ is the rate of VR from state $|b\rangle$ to state $|b'\rangle$. γ_b is the total decay rate of level $|b\rangle$, consisting of a VR part and a radiative part (γ_r). Equation (119c) is the detailed balance condition, which guarantees that the system will evolve to thermal equilibrium at long times. Finally, Eq. (119d) accounts for the decay of coherences due to the relaxation matrix. The relaxation matrix [Eqs. (119)] corresponds to the following equations of motion:

$$\frac{d\rho_{bb}}{dt} = -\gamma_b \rho_{bb} + \sum_{b' \neq b} \gamma_{bb'} \rho_{b'b'}, \tag{120a}$$

which can be written in a matrix form

$$\frac{d\boldsymbol{\rho}}{dt} = -\hat{\gamma}\boldsymbol{\rho}, \tag{120b}$$

where $\boldsymbol{\rho}$ is a vector, whose components are ρ_{bb}. The equation of motion for the coherences, corresponding to Eq. (119d), is

$$\frac{d\rho_{bb'}}{dt} = -\Gamma_{bb'} \rho_{bb'}, \qquad b \neq b'. \tag{120c}$$

Making use of Eqs. (118) and (119), we can solve for the SRF lineshapes by repeating the procedure of Sections V and VI. The final result is[59,96]

$$S_{\mathrm{SRF}}(\omega_1, \omega_2) = S_{\mathrm{RAMAN}}(\omega_1, \omega_2) + S_{\mathrm{FL}}(\omega_1, \omega_2), \tag{121a}$$

where

$$S_{\mathrm{RAMAN}}(\omega_1, \omega_2) = 2\pi \sum_{a,c} P(a)|K_{ca}(\varepsilon_a + \omega_1)|^2 \delta(\omega_1 - \omega_2 - \omega_{ca}), \tag{121b}$$

$$S_{\mathrm{FL}}(\omega_1, \omega_2) = S^{\mathrm{I}}_{\mathrm{FL}}(\omega_1, \omega_2) + S^{\mathrm{II}}_{\mathrm{FL}}(\omega_1, \omega_2) + S^{\mathrm{III}}_{\mathrm{FL}}(\omega_1, \omega_2), \tag{121c}$$

$$S^{\mathrm{I}}_{\mathrm{FL}}(\omega_1, \omega_2) = 4 \sum_{b',b} [\mathrm{Im}\, \bar{K}_{b'b}(\varepsilon_{b'} - \omega_2)](\hat{\gamma}^{-1})_{b'b}[\mathrm{Im}\, \bar{K}_{bb}(\varepsilon_b - \omega_1)], \tag{121d}$$

$$S_{FL}^{II}(\omega_1,\omega_2) = 2\,\mathrm{Im}\sum_{b\neq d}\frac{[\bar{K}_{bd}(\varepsilon_b-\omega_2)-\bar{K}^*_{db}(\varepsilon_d-\omega_2)]\bar{K}_{db}(\varepsilon_b-\omega_1)}{\omega_{db}+i\Gamma_{db}}, \tag{121e}$$

$$S_{FL}^{III}(\omega_1,\omega_2) = 2\,\mathrm{Im}\sum_{a,c}P(a)\,\mathrm{PP}\frac{K_{ca}(\varepsilon_c+\omega_2)K^*_{ca}(\varepsilon_a+\omega_1)}{\omega_1-\omega_2-\omega_{ca}}. \tag{121f}$$

Here K, $\bar{K}$, and $\hat{K}$ are given by Eqs. (81). The definition of $T(t)$ now need to be changed. Previously, all levels had the same lifetime. Now we have

$$T_{ca}(t) = \sum_b V_{cb}\exp(-i\varepsilon_b t - \tfrac{1}{2}\gamma_b t)V_{ba}J_a(t). \tag{122}$$

In the absence of VR, $\gamma_b = \gamma_r$, and Eq. (122) reduces to Eq. (79) with $\gamma = \gamma_r$. The off-diagonal terms ($b' \neq b$) in S_{FL}^{I} are induced by the VR. The nature of this term is determined by the relative magnitude of the VR rates $\gamma_{b'b}$ and the radiative lifetime γ_r.[59,96] In the slow VR limit $\gamma_r \gg \gamma_{b'b}$, we have

$$(\hat{\gamma}^{-1})_{b'b} = \gamma_r^{-1}\delta_{bb'}. \tag{123}$$

In this case, Eq. (121) reduce to Eq. (84). In the opposite (fast VR) limit, $\gamma_{b'b} \gg \gamma_r$, and we can analyze Eq. (121) as follows. Since $\hat{\gamma}$ is non-Hermitian its left ($\langle\lambda_i|$) and right ($|\lambda_i\rangle$) eigenvectors are not the same. The left and right eigenvalues λ_i are, however, identical. We then have

$$\hat{\gamma}|\lambda_i\rangle = \lambda_i|\lambda_i\rangle, \tag{124a}$$

$$\langle\lambda_i|\hat{\gamma} = \lambda_i\langle\lambda_i|. \tag{124b}$$

and

$$\hat{\gamma}^{-1} = \sum_i \frac{|\lambda_i\rangle\langle\lambda_i|}{\lambda_i}. \tag{124c}$$

Let us now consider the $\hat{\gamma}$ matrix in the absence of radiative lifetime ($\gamma_r = 0$). In that case, it has an equilibrium vector with eigenvalue $\lambda_0 = 0$, that is,

$$|\lambda_0\rangle = \sum_b \sigma_e(b)|b\rangle, \tag{125a}$$

$$\langle\lambda_0| = \sum_b \langle b|, \tag{125b}$$

where $\sigma_e(b)$ is the equilibrium distribution of $|b\rangle$ in the electronically excited

state [Eq. (46a)], that is,

$$\sigma_e(b) = \exp(-\varepsilon_b/kT) \Big/ \sum_b \exp(-\varepsilon_b/kT). \tag{126}$$

All other eigenvectors $|\lambda_i\rangle$ will have eigenvalues $O(\gamma_{b'b})$. When $\gamma_{b'b} \gg \gamma_r$, we can treat γ_r perturbatively. Using first-order perturbation theory, we have

$$\lambda_0 \cong \gamma_r, \tag{127a}$$

$$\lambda_i \cong \gamma_{b'b} + O(\gamma_r), \qquad i = 1, 2, \ldots. \tag{127b}$$

We thus have separation of time scales and $\lambda_0 \ll \lambda_i$, $i \neq 0$. λ_0 will then be dominant in Eq. (124c), resulting in

$$\mathfrak{f}^{-1} \cong \frac{|\lambda_0\rangle\langle\lambda_0|}{\lambda_0}, \tag{128a}$$

that is,

$$\mathfrak{f}^{-1} = \sum_{b,b'} \frac{\sigma_e(b')|b'\rangle\langle b|}{\gamma_r}. \tag{128b}$$

S^1_{FL} thus assumes the form

$$S^1_{FL}(\omega_1, \omega_2) = \frac{4}{\gamma_r} \sum_{b'} \sigma_e(b')[\operatorname{Im} \bar{K}_{b'b'}(\varepsilon_{b'} - \omega_2)] \sum_b [\operatorname{Im} \bar{K}_{bb}(\varepsilon_b - \omega_1)]. \tag{129}$$

This corresponds to "fully relaxed" emission coming from the equilibrated distribution of vibronic states. Equation (121) thus interpolates between the previous expression, Eq. (84), which contains no VR, and the fast relaxation limit, Eq. (129), whereby the emission is fully relaxed. The key parameter controlling this behavior is $\gamma_{b'b}/\gamma_r$.

The role of vibrational relaxation and solvation dynamics can be probed most effectively by fluorescence experiments, which are both time- and frequency-resolved,[66-68] as indicated at the end of Sec. V. We have recently developed a theory for fluorescence of polar molecules in polar solvents.[68] The solvaion dynamics is related to the solvent dielectric function $\varepsilon(\omega)$ by introducing a solvation coordinate. When $\varepsilon(\omega)$ has a Lorentzian dependence on frequency (the Debye model), the broadening is described by the stochastic model [Eqs. (113)], where the parameters Δ and Λ may be related to molecular

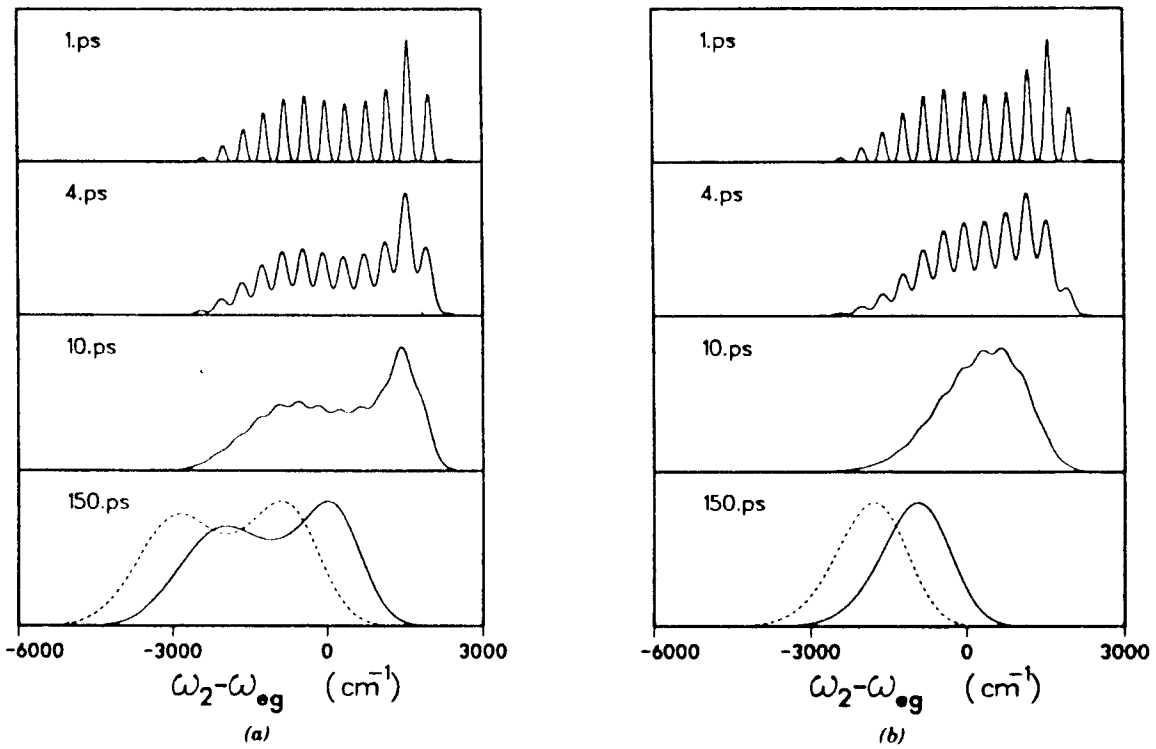

Figure 17. Time-resolved fluorescence spectra of a solute with one vibrational mode in ethanol at 247 K.[68] The various frames show the fluorescence spectrum measured at successively later times after the application of a 1 ps excitation pulse. Each spectrum is labeled with the observation time. The steady-state fluorescence spectrum is given by the dashed curve in the bottom frame. In the electronic ground state, the solute vibrational frequency is 400 cm^{-1}, and in the excited state, the frequency is 380 cm^{-1}. The dimensionless displacement is 1.4. The permanent dipole moment changes by 10 Debye upon electronic excitation. The Onsager radius is 3Å. The longitudinal dielectric relaxation time, τ_L, is 150 ps. $\omega_1 - \omega_{eg} = 2000$ cm^{-1}. (a) Vibrational relaxation is not included. (b) Finite vibrational relaxation rate of $\gamma = 25/\tau_L = 0.167$ $psec^{-1}$ is included.

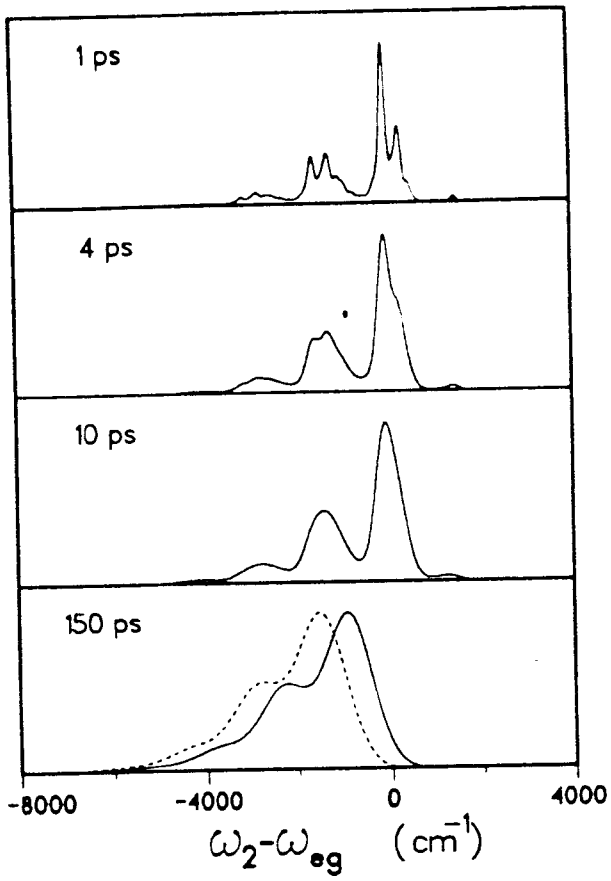

Figure 18. Time-resolved fluorescence spectra of a polyatomic solute in ethanol at 247 K following a 1 ps excitation pulse.[68] The model solute has the 29 Raman active vibrational modes of the retinal chromophore in bacteriorhodopsin and undergoes rapid vibrational relaxation. $\omega_1' - \omega_{ee} = 1528\ cm^{-1}$. The solvent and the broadening parameters are the same as used in Fig. 17.

and solvent properties. In addition, the model exhibits a time-dependent solvent shift which reflects the solvent reorganization. We have also incorporated vibrational relaxation using the master equation introduced in this section. In Fig. 17, we display the time-resolved fluorescence spectrum of a model solute with one harmonic vibrational mode, calculated by using Eq. (76). Fig. 17a is calculated in the absence of vibrational relaxation and reflects the solvation dynamics. In Fig. 17b, a finite vibrational relaxation rate is included. In Fig. 18, we show a similar calculation for the retinal chromophore in bacteriorhodopsin with 29 vibrational modes. Fast vibrational relaxation

was assumed in this calculation, which used our eigenstate-free procedure. These spectra are narrow at short times due to the capability of the excitation process to select a subgroup of solvent configurations. As time evolves, a broadening and red shift take place, which reflect the solvent reorganization process. Time- and frequency-resolved fluorescence lineshapes thus provide a unique probe for solvation dynamics on microscopic length scales and time scales.

IX. INTRAMOLECULAR VIBRATIONAL REDISTRIBUTION (IVR) IN ULTRACOLD MOLECULES IN SUPERSONIC BEAMS

The calculation of molecular fluorescence and Raman spectra in large anharmonic molecules is one of the fundamental problems in molecular dynamics and spectroscopy. Recent experiments, particularly involving ultracold molecules in supersonic beams,[60,98-102] are yielding accurate and detailed information (both time-resolved and frequency-resolved). In the previous sections we demonstrated how correlation function techniques, which are based on a *reduced description*, may be used to calculate SRF and 4WM lineshapes in macroscropic systems. The reduced correlation function formulation allows us to calculate any lineshape function without attempting to calculate the exact eigenstates of the macroscopic system. Calculating the eigenstates of a macroscopic system is extremely difficult owing to the large number of degrees of freedom involved. Moreover, the experimental broad line-shapes contain highly averaged information and do not reveal properties of individual eigenstates. The calculation of individual eigenstates of macroscopic systems is therefore neither feasible nor desirable. The analysis of spectra of isolated molecules is, on the other hand, traditionally made in terms of properties of individual molecular eigenstates (level positions and dipole matrix elements).[103] Such an approach is appropriate for small or intermediate size molecules, but for large molecules (10 atoms or more), it is impractical. The spectra show intramolecular line broadening in which information on individual eigenstates is highly averaged. This situation is reminiscent of the behavior of macroscopic systems, and it seems natural to adopt the techniques developed in the previous sections toward the treatment of intramolecular line broadening in large isolated polyatomic molecules.

In order to develop a reduced description for the spectroscopy of ultracold, isolated molecules in supersonic beams, we partition the molecular vibrational degrees of freedom into a few "system" modes, which are strongly coupled to the electronic transition of interest and are characterized by large values

of the displacements D_j, and the rest of the vibrational degrees of freedom are treated as an intramolecular bath.[59,61,102] Once we have identified the "system" modes and the "bath" modes, the calculation of SRF lineshapes of ultracold molecules may be carried out using the formulation developed in Sections V and VIII. There are several points that make this calculation quite different from SRF in solution. First, the incident frequency is usually tuned to a narrow, isolated vibronic level in the electronically excited state. This state serves as a *doorway state*,[102] and its contribution is dominant in the emission. An excellent approximation will therefore be to eliminate the summation over intermediate states $|b\rangle$ and $|d\rangle$ in Eq. (78) and consider a single doorway state $|b\rangle$. This simplifies the calculation considerably. Another fundamental difference exists between the intramolecular bath and the solvent treated in previous sections. The solvent has an infinite number of degrees of freedom, and it is normally at a finite temperature. It is therefore reasonable to assume that its motions are very weakly correlated with the state of the system. This enabled us to use the projection operator Eq. (58) and the factorization approximation. For isolated polyatomic molecules (say anthracene or di-fluorobenzene), the situation is very different. The bath is finite and is initially cold ($T = 0°K$). As the vibrational relaxation proceeds, the excess vibrational energy is released into the bath. *The state of the bath is therefore strongly correlated with the vibronic state of the system.* A reduced description of the emission can then be obtained by introducing the following projection operator[59,61]

$$\hat{P} = |gg\rangle\rangle\langle\langle gg|\rho_g \mathrm{Tr}_B + \sum_b |bb\rangle\rangle\langle\langle bb|\rho_e^b \mathrm{Tr}_B. \tag{130}$$

The ground-state projection $|gg\rangle\rangle\langle\langle gg|$ is identical to Eq. (58), and ρ_g is, in this case, the zero-temperature density matrix of the bath. For the excited state, we define ρ_e^b as the bath density matrix, when the system is in the $|b\rangle$ state. As the vibrational relaxation proceeds, the bath energy increases, and ρ_e^b changes. A simple way to model ρ_e^b is by assuming a harmonic bath with a microcanonical distribution. Note that the previous projection operator [Eq. (58)] is a special case of Eq. (130) obtained by taking ρ_e^b to be independent of $|b\rangle$. This is the case for an infinite bath that is weakly correlated with the state of the system. Our procedure for incorporating the effects of IVR processes on the emission lineshapes of supercooled molecules is based on introducing an IVR rate $\gamma_{b'b}$, whereby the doorway state $|b\rangle$ relaxes to state $|b'\rangle$ (see Section VIII). Once the system is in the $|b'\rangle$ state, the bath modes become hot, since they absorb the excess vibrational energy $\omega_{bb'}$. As a result, the emission from the $|b'\rangle$ state can be represented by our stochastic model, whereby the parameters Δ and Λ [Eq. (113)] now depend on the amount of

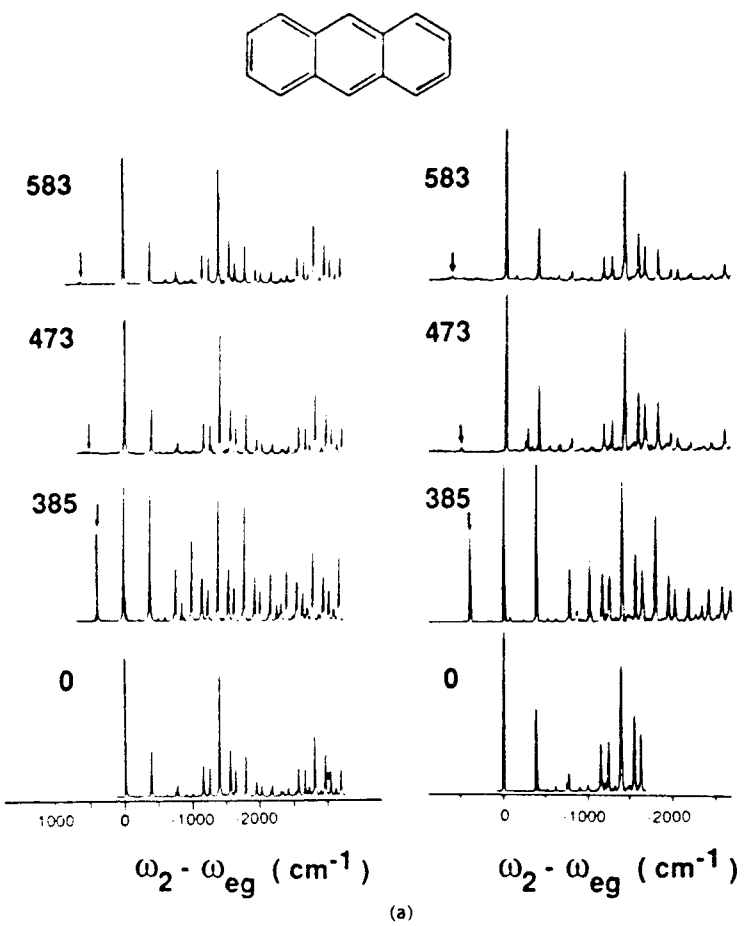

Figure 19. Dispersed fluorescence of ultracold anthracene in a supersonic beam for several values of the excess vibrational energy, which is indicated (in cm^{-1}) on each plot. The right column is experimental,[60] and the left column is our 17-mode harmonic calculation (Table II).[61] The agreement is excellent at low excitation energies ($< 766\ cm^{-1}$), but fails at higher energies owing to the onset of IVR processes.

vibrational energy in the bath. For the doorway state $|b\rangle$, $\Delta = 0$, and there is no broadening. We expect that the stochastic fluctuation amplitude Δ for emission from a given $|b'\rangle$ state will increase as the available vibrational energy of the bath $\omega_{bb'}$ increases. The total emission thus consists of a progression of narrow lines originating from the doorway state and a series of broad emission lines corresponding to the redistributed emission. Our expression for the emission, in this case, is[61]

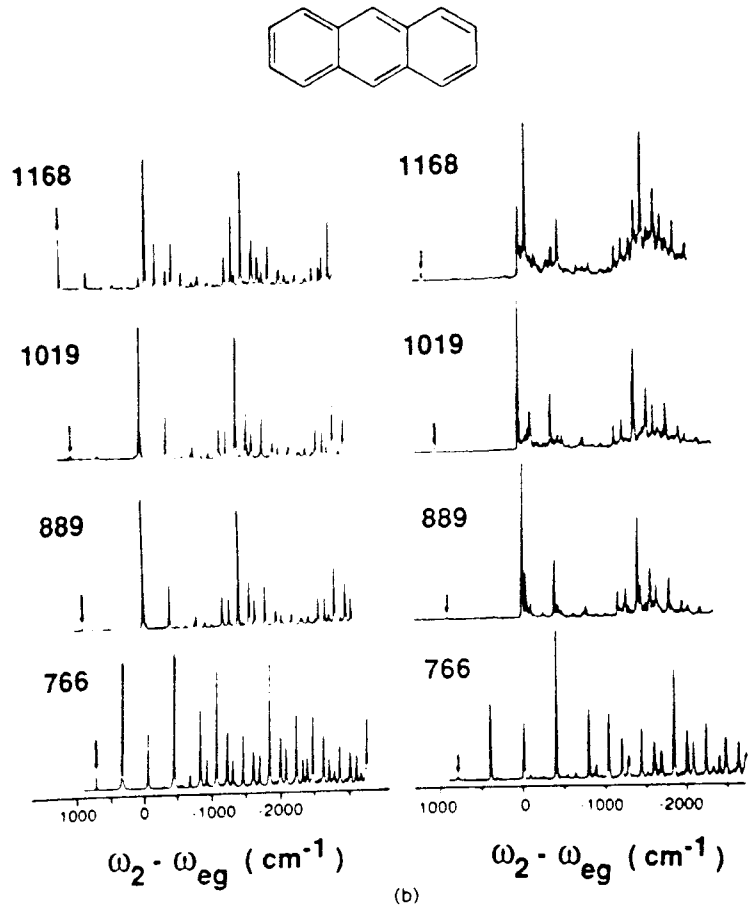

(b)

Figure 19 (*continued*)

$$S_{SRF}(\omega_1, \omega_2) = \frac{-2\gamma_b |\mu_{ba}|^2}{(\omega_1 - \omega_{ba})^2 + (\gamma_b/2)^2} \sum_{b'} (\gamma^{-1})_{b'b} [\mathrm{Im}\, \bar{K}_{b'b}(\varepsilon_{b'} - \omega_2)], \quad (131)$$

where $\bar{K}_{b'b}$ is given by Eqs. (79) and (81) together with Eq. (114), and the bath parameters Δ and Λ are taken to be dependent on $|b'\rangle$. Equation (131) is a special case of $S^{\mathrm{I}}_{\mathrm{FL}}(\omega_1, \omega_2)$ [Eq. (121d)]. We have applied Eq. (131) toward the calculation of the emission spectra of ultracold anthracene. A comprehensive supersonic beam study of this molecule was conducted recently by Zewail and co-workers.[60] Our results are displayed in Figs. 19–21. Anthracene has 17 system modes that are strongly coupled to the electronic transition. The parameters of these modes used on our calculation are summarized in Table II.

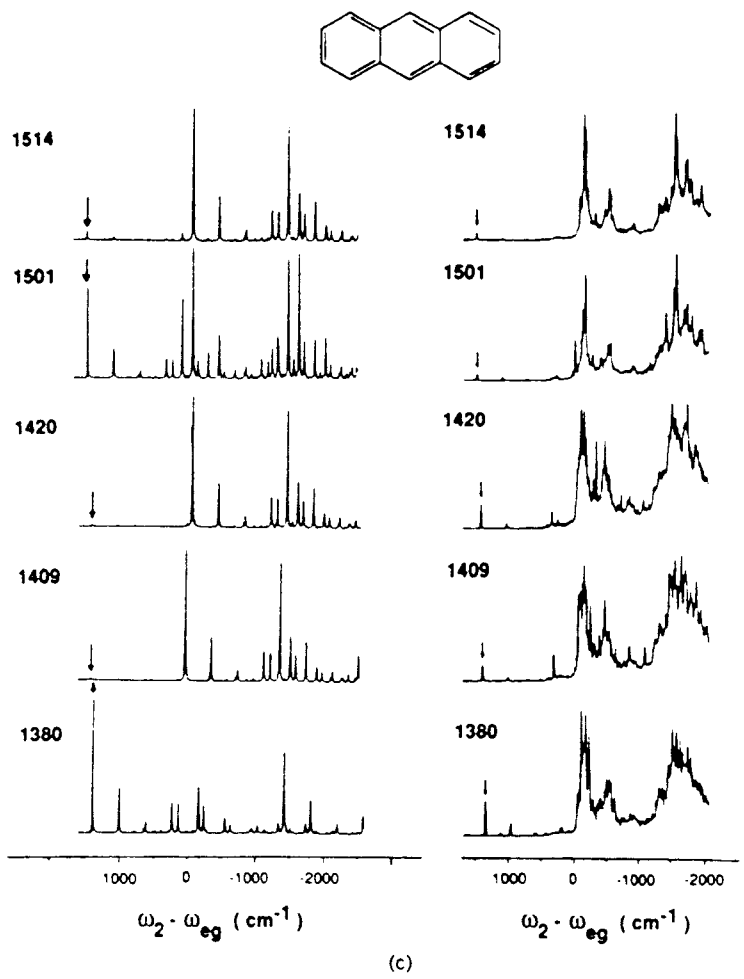

(c)

Figure 19 (*continued*)

In Fig. 19, we compare the calculated emission spectra in the harmonic limit (no vibrational relaxation) with experiment. At low excess vibrational energy (< 766 cm^{-1}), the agreement is excellent. At higher energies. the harmonic calculations fail to reproduce the broad redistributed emission, which becomes increasingly dominant with increasing excess energy. The redistributed emission can be quantitatively accounted for by incorporating the IVR processes via Eq. (131). Figure 20 focuses on excess vibrational energy of 1792 cm^{-1} in which IVR processes play an important role in the emission. since the purely harmonic emission (bottom figure) clearly fails to reproduce

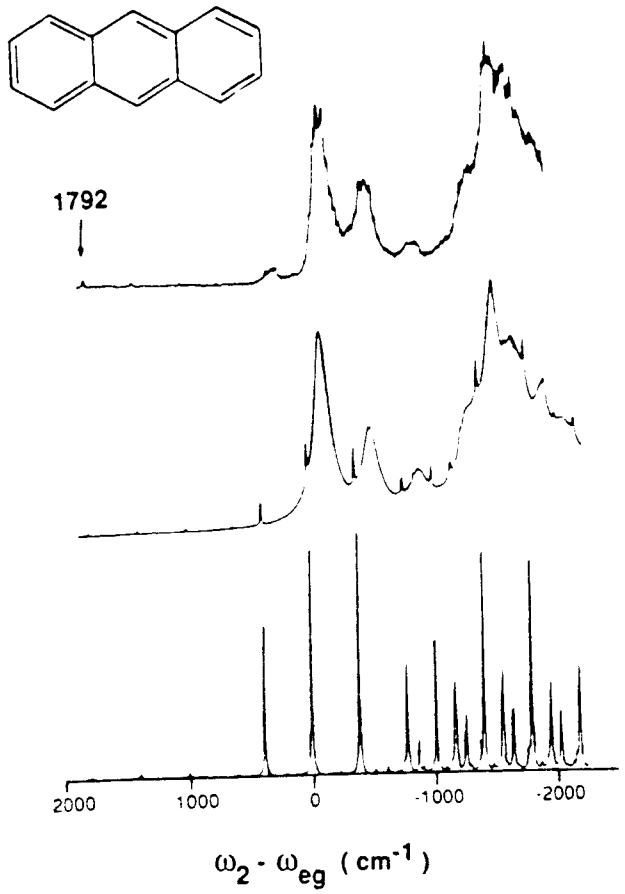

Figure 20. $\bar{5}_0^1 12_0^1$ dispersed fluorescence of ultracold anthracene in a supersonic beam. The available vibrational energy is 1792 cm^{-1}. The parameters of the optically active modes are given in Table II. The top figure is the experimental spectrum.[60] The bottom figure is the emission in the harmonic approximation ($\gamma_{b'b} = 0$). The calculation clearly fails to reproduce the broad redistributed emission. The middle figure was calculated with IVR [Eqs. (131)]. Only one $|b'\rangle$ state (the ground vibrational state $|b'\rangle = |0\rangle$) was used. $\gamma_{b'b}/\gamma_r = 40$. The relaxed emission was calculated in the fast modulation limit [Eq. (116a)], with $\Gamma_0 = 2\hat{\Gamma} = 75\ cm^{-1}$.[61]

the broad experimental spectrum (top figure). The middle figure, which introduced IVR via our stochastic model [Eq. (131)], adequately reproduces the experimental spectrum. This effect becomes more dramatic as the excess vibrational energy is increased. Figure 20 was calculated in the fast modulation (Lorentzian) limit [Eq. (116a)]. Finally, Fig. 21 shows the calculated emission spectrum of vibrationally hot anthracene at three temperatures. This calcula-

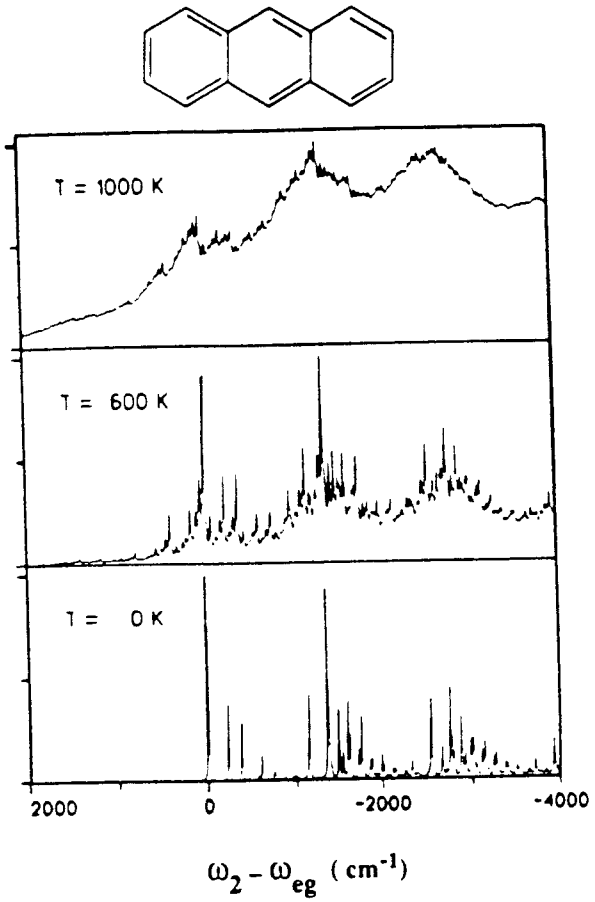

Figure 21. The total emission spectrum of anthracene at finite temperatures,[61] taking the electronically excited state to be in thermal equilibrium at three different temperatures [Eq. (46a)]. The calculation was made using Eq. (131), with a linewidth $\Gamma_0 = 2\Gamma = 10\ cm^{-1}$.

tion was made in the harmonic limit in the absence of IVR processes. The present calculations demonstrate the simplicity in which this model can be used to interpret the spectra of large polyatomic molecules and molecular clusters.[99,104] The amount of computational effort does not increase dramatically as the molecular size increases. This is in sharp contrast to conventional expressions, based on summations over eigenstates of the system and the bath, which are intractable for large molecules. Methods for controlling IVR processes in SRF lineshapes were discussed recently.[105] The effects of

TABLE II
Frequencies and Dimensionless Displacements of Anthracene[60,61]

Mode	ω_j (cm^{-1})	ω_j (cm^{-1})	D_j
12	390	385	0.79
11	624	583	0.21
10	753	755	0.24
9	1012	1019	0.20
8	1165	1163	0.67
7	1263	1168	0.69
6	1408	1380	1.35
5	1486	1420	0.20
4	1566	1501	0.80
$\bar{11}$	391	232	0.33
$\bar{10}$	524	473	0.15
$\bar{9}$	912	889	0.20
$\bar{8}$	1100	1046	0.15
$\bar{7}$	1184	1183	0.24
$\bar{5}$	1382	1409	0.20
$\bar{4}$	1576	1514	0.35
$\bar{3}$	1643	1635	0.63

incoherence in the radiation field on SRF[106] and 4WM[63] lineshapes may also be analyzed using the present formalism.

X. AN EIGENSTATE-FREE EXPRESSION FOR THE NONLINEAR RESPONSE FUNCTION

In the previous sections, we have utilized Green's function techniques to eliminate some of the summations involved in the calculations of nonlinear susceptibilities. The general expression for $R(t_3, t_2, t_1)$ [Eq. (49) or (60)], involves four summations over molecular states a, b, c, d. In Eq. (80) we carried out two of these summations for harmonic molecules. It should be noted that for this particular model it is possible to carry out formally all the summations involved, resulting in a closed time-domain expression for $R(t_3, t_2, t_1)$. This expression, however, cannot be written in terms of simple products of functions of t_1, t_2, and t_3. Therefore, calculating the frequency-domain response function $\hat{R}$ via Eq. (30) requires the performing of a triple Fourier transform (rather than three one-dimensional transforms). This formula is, therefore, useful for extremely short pulses when a time-domain expression is needed. Otherwise, it is more convenient to use the expressions of Section VI, whereby only two of the four summations were carried out, but the transformation to

the frequency domain is much simpler. We have shown that the response function contains eight terms (Fig. 6). We can express each term using the four-point correlation function of the dipole operator, $F(t_1,t_2,t_3,t_4)$, Eq. (54). We have recently evaluated F for our harmonic model [Eq. (85)] in the absence of Dushinsky rotation.[64] In this case, the four-point correlation function F can be factorized as a product of terms corresponding to the various modes:

$$F(t_1,t_2,t_3,t_4)=\prod_{j=1}^{N} F_j(t_1,t_2,t_3,t_4), \tag{132}$$

making use of the Condon approximation [Eq. (89)], and assuming that the ground and the excited state frequencies are the same $\omega_j'=\omega_j''\equiv\omega_j$, we get

$$F_j(t_1,t_2,t_3,t_4)=\exp[(D_j^2/2)(f_j+\bar{f}_j-\bar{n}_j f_j f_j^*)], \tag{133a}$$

where

$$f_j=\exp[-i\omega_j(t_1-t_4)]-\exp[-i\omega_j(t_2-t_4)]-\exp[-i\omega_j(t_3-t_4)]-1, \tag{133b}$$

$$\bar{f}_j=\exp[-i\omega_j(t_1-t_2)]-\exp[-i\omega_j(t_1-t_3)]-\exp[-i\omega_j(t_2-t_3)]-1, \tag{133c}$$

and

$$\bar{n}_j=[\exp(\hbar\omega_j/kT)-1]^{-1}. \tag{133d}$$

$F(t_1,t_2,t_3,t_4)$ can be calculated for the general harmonic model [Eq. (85)] with $\omega_j'\neq\omega_j''$ by using the methodology developed in Ref. 58. For anharmonic systems, it may be possible to calculate $F(t_1,t_2,t_3,t_4)$ approximately by making use of a semiclassical propagation scheme in Liouville space.[107]

XI. CONCLUDING REMARKS

In this chapter, we developed a general theory of 4WM processes in terms of the nonlinear response function of the nonlinear medium $R(t_3,t_2,t_1)$. The response function is an intrinsic molecular property that contains all the microscopic information relevant to any type of 4WM process. The details of a particular 4WM experiment are contained in the external fields $E_1(t)$, $E_2(t)$, $E_3(t)$, and in the particular choice of the observable mode $\mathbf{k}_s$. The generated signal is calculated by convolving the response function with the external fields and choosing $\mathbf{k}_s$ [Eqs. (27), (28), and (31)]. It is only at this stage that

the distinction among the various 4WM techniques (photon echo, transient grating, CARS, CSRS, etc.) is made. We have further shown that SRF lineshapes may be expressed in terms of the same four-point correlation function of the dipole operator that is required for the description of 4WM processes. Microscopic and stochastic models and approximation schemes for the explicit evaluation of these lineshapes for polyatomic molecules in condensed phases and in supersonic beams were developed and analyzed.

Acknowledgments

The support of the National Science Foundation, the Office of Naval Research, the U.S. Army Research Office, the Petroleum Research Fund, administered by the American Chemical Society, and the Camille and Henry Dreyfus Foundation is gratefully acknowledged. I wish to thank Z. Deng, R. F. Loring, K. Shan, J. Sue, and Y. J. Yan for stimulating discussions. The critical comments of A. H. Zewail are most appreciated. Special thanks go to Irmhild O. Barnett for the careful typing.

References

1. N. Bloembergen, *Nonlinear Optics*. Benjamin, New York, 1965.
2. P. N. Butcher, *Nonlinear Optical Phenomena*. Ohio University Press, Athens, Ohio, 1965.
3. S. A. J. Druet and J. P. E. Taran, *Progr. Quantum Electron.* **7**, 1 (1981).
4. Y. R. Shen, *The Principles of Nonlinear Optics*. Wiley, New York, 1984.
5. G. R. Fleming, *Chemical Applications of Ultrafast Spectroscopy*. Oxford, London, 1986.
6. S. Mukamel and R. F. Loring, *J. Opt. Soc. Am. B* **3**, 595 (1986).
7. J. Tang and A. C. Albrecht, in *Raman Spectroscopy* (H. A. Szymanski, ed.). Plenum, New York, 1970, Vol 2, p. 33; P. M. Champion and A. C. Albrecht, *Annu. Rev. Phys. Chem.* **333**, 353 (1982).
8. B. Johnson and W. Peticolas, *Annu. Rev. Phys. Chem.* **27**, 465 (1976); L. Chinsky, A. Laigle, W. L. Peticolas, and P. Y. Turpin, *J. Chem. Phys.* **76**, 1 (1982).
9. T. G. Spiro, *Adv. Protein Chem.* **37**, 111 (1985).
10. A. B. Myers and R. A. Mathies, in *Biological Applications of Raman Spectroscopy*, Vol. 2 (T. G. Spiro, ed.). Wiley, N.Y. 1987, p. 1.
11. S. Mukamel, *Phys. Reports* **93**, 1 (1982).
12. S. Mukamel, *J. Phys. Chem.* **88**, 3185 (1984).
13. N. Bloembergen, H. Lotem, and R. T. Lynch, *Indian J. Pure Appl. Phys.* **16**, 151 (1978).
14. T. K. Yee and T. K. Gustafson, *Phys. Rev. A* **18**, 1597 (1978).
15. J. L. Oudar and Y. R. Shen, *Phys. Rev. A* **22**, 1141 (1980).
16. Y. Prior, A. R. Bogdan, M. Dagenais, and N. Bloembergen, *Phys. Rev. Lett.* **46**, 111 (1981); A. R. Bogdan, M. W. Downer, and N. Bloembergen, *Phys. Rev. A* **24**, 623 (1981); L. J. Rothberg and N. Bloembergen, *Phys. Rev. A* **30**, 820 (1984).
17. J. R. Andrews and R. M. Hochstrasser, *Chem. Phys. Lett.* **82**, 381 (1981); J. R. Andrews, R. M. Hochstrasser, and H. P. Trommsdorff, *Chem. Phys.* **62**, 87 (1981).
18. T. Yajima and H. Souma, *Phys. Rev. A* **17**, 309 (1978), T. Yajima, H. Souma, and Y. Ishida, *Phys. Rev. A* **17**, 324 (1978).
19. S Mukamel, *Phys. Rev. A* **28**, 3480 (1983).
20. R. W. Boyd and S. Mukamel, *Phys. Rev. A* **29**, 1973 (1984).
21. V. Mizrahi, Y. Prior, and S. Mukamel, *Opt. Lett.* **8**, 145 (1983).
22. I. D. Abella, N. A. Kurnit, and S. R. Hartmann, *Phys. Rev.* **141**, 391 (1966); S. R. Hartmann,

IEEE J. Quantum Electron. **4**, 802 (1968); T. W. Mossberg, R. Kachru, A. M. Flusberg, and S. R. Hartmann, *Phys. Rev. A* **20**, 1976 (1979).
23. H. W. Hesselink and D. A. Wiersma, in *Modern Problems in Condensed Matter Sciences*, (V. M. Agranovich and A. A. Maradudin, eds.). North-Holland, Amsterdam, 1983, Vol. 4, p. 249.
24. R. W. Olson, F. G. Patterson, H. W. H. Lee, and M. D. Fayer, *Chem. Phys. Lett.* **78**, 403 (1981).
25. R. F. Loring and S. Mukamel, *Chem. Phys. Lett.* **114**, 426 (1985).
26. J. R. Salcedo, A. E. Siegman, D. D. Dlott, and M. D. Fayer, *Phys. Rev. Lett.* **41**, 131 (1978).
27. M. D. Fayer, *Ann. Rev. Phys. Chem.* **33**, 63 (1982).
28. P. F. Liao, L. M. Humphrey, and D. M. Bloom, *Phys. Rev. B* **10**, 4145 (1979).
29. J. K. Tyminski, R. C. Powell, and W. K. Zwicker, *Phys. Rev. B* **29**, 6074 (1984).
30. H. J. Eichler, *Optica Acta* **24**, 631 (1977).
31. A. von Jena and H. E. Lessing, *Opt. Quant. Electron.* **11**, 419 (1979).
32. D. K. Garrity and J. L. Skinner, *J. Chem. Phys.* **82**, 260 (1985).
33. R. F. Loring and S. Mukamel, *J. Chem. Phys.* **83**, 4353 (1985); **84**, 1228 (1985); **85**, 1950 (1986).
34. N. Bloembergen, *Am. J. Phys.* **35**, 989 (1967).
35. A. Laubereau and W. Kaiser, *Rev. Mod. Phys.* **50**, 607 (1978); W. Zinth, H. J. Polland, A. Laubereau, and W. Kaiser, *Appl. Phys. B* **26**, 77 (1981).
36. S. M. George, A. L. Harris, M. Berg, and C. B. Harris, *J. Chem. Phys.* **80**, 83 (1984).
37. I. I. Abram, R. M. Hochstrasser, J. E. Kohl, M. G. Semack, and D. White, *J. Chem. Phys.* **71**, 153 (1979); F. Ho, W. S. Tsay, J. Trout, S. Velsko, and R. M. Hochstrasser, *Chem. Phys. Lett.* **97**, 141 (1983).
38. E. L. Chronister and D. D. Dlott, *J. Chem. Phys.* **79**, 5286 (1984); C. L. Schosser and D. D. Dlott, *J. Chem. Phys.* **80**, 1394 (1984).
39. B. H. Hesp and D. A. Wiersma, *Chem. Phys. Lett.* **75**, 423 (1980); D. P. Weitekamp, K. Duppen, and D. A. Wiersma, *Phys. Rev. A* **27**, 3089 (1983).
40. A. M. Weiner, S. DeSilvestri, and E. P. Ippen, *J. Opt. Soc. Am. B* **2**, 654 (1985).
41. B. S. Hudson, W. H. Hetherington, S. P. Cramer, I. Chabay, and G. K. Klauminzer, *Proc. Nat'l. Acad. Sci. (USA)* **73**, 3798 (1976).
42. L. A. Carreira, T. C. Maguire, and T. B. Malloy, *J. Chem. Phys.* **66**, 2621 (1977).
43. R. F. Loring and S. Mukamel, *J. Chem. Phys.* **83**, 2116 (1985).
44. S. Mukamel, *J. Chem. Phys.* **82**, 5398 (1985); J. Sue, Y. J. Yan, and S. Mukamel, *J. Chem. Phys.* **85**, 462 (1986).
45. Z. Deng and S. Mukamel, *J. Chem. Phys.* **85**, 1738 (1986).
46. O. Brafman, C. K. Chan, B. Khodadoost, J. B. Page, and C. T. Walker, *J. Chem. Phys.* **80**, 5406 (1984); C. K. Chan, J. B. Page, D. L. Tonks, O. Brafman, B. Khodadoost, and C. T. Walker, *J. Chem. Phys.* **82**, 4813 (1985).
47. F. Inagaki, M. Tasumi, and T. Miyazawa, *J. Mol. Spectrosc.* **50**, 286 (1974); S. Saito, M. Tasumi, and C. H. Eugster, *J. Raman Spectrosc.* **14**, 299 (1983); S. Saito and M. Tasumi, *J. Raman Spectrosc.* **14**, 310 (1983).
48. J. B. Page and D. L. Tonks, *J. Chem. Phys.* **75**, 5694 (1981); C. K. Chan and J. B. Page, *J. Chem. Phys.* **79**, 5234 (1983); *Chem. Phys. Lett.* **104**, 609 (1984).
49. T. Kitagawa, M. Abe, and H. Ogoshi, *J. Chem. Phys.* **69**, 4516 (1978); M. Abe, T. Kitagawa, and Y. Kyogoku, *J. Chem. Phys.* **69**, 4526 (1978).
50. B. E. Kohler, T. A. Spiglanin, R. J. Hemley, and M. Karplus, *J. Chem. Phys.* **80**, 23 (1984); J. R. Ackerman, S. A. Forman, H. Hossain, and B. E. Kohler, *J. Chem. Phys.* **80**, 39 (1984).
51. A. Warshel, *Annu. Rev. Biophys. Bioeng.* **6**, 273 (1977); A. Warshel and P. Dauber, *J. Chem. Phys.* **66**, 5477 (1977).

52. B. S. Hudson, B. E. Kohler, and K. Schulten, in *Excited States*, Vol. 6 (E. C. Lim, ed.). Academic, New York, 1982, p. 1.
53. B. R. Stallard, P. M. Champion, P. R. Collis, and A. C. Albrecht, *J. Chem. Phys.* **78**, 712 (1983); D. Lee, B. R. Stallard, P. M. Champion, and A. C. Albrecht, *J. Phys. Chem.* **88**, 6693 (1984).
54. Z. Z. Ho, R. C. Hanson, and S. H. Lin, *J. Chem. Phys.* **77**, 3414 (1982); Z. Z. Ho, T. A. Moore, S. H. Lin, and R. C. Hanson, *J. Chem. Phys.* **74**, 873 (1981); Z. Z. Ho, R. C. Hanson, and S. H. Lin, *J. Phys. Chem.* **89**, 1014 (1985).
55. W. Siebrand and M. Z. Zgierski, *J. Chem. Phys.* **71**, 3561 (1979); in *Excited States*, (E. C. Lim, ed.). Academic, New York, 1979, Vol. 4, p. 1; W. Siebrand and M. Z. Zgierski, *J. Chem. Phys.* **71**, 3561 (1979).
56. A. B. Myers, R. A. Harris, and R. A. Mathies, *J. Chem. Phys.* **79**, 603 (1983).
57. S. Mukamel, *J. Chem. Phys.* **71**, 2884 (1979).
58. S. Mukamel, S. Abe, Y. J. Yan, and R. Islampour, *J. Phys. Chem.* **89**, 201 (1985); Y. J. Yan and S. Mukamel, *J. Chen Phys.* **85**, 5908 (1986).
59. S. Mukamel and R. E. Smalley, *J. Chem. Phys.* **73**, 4156 (1980).
60. W. R. Lambert, P. M. Felker, and A. H. Zewail, *J. Chem. Phys.* **81**, 2209 (1984); **81**, 2195 (1984); **81**, 2217 (1984); W. R. Lambert and A. H. Zewail, *J. Chem. Phys.* **82**, 3003 (1985); P. M. Felker and A. H. Zewail, *J. Chem. Phys.* **82**, 2961 (1985); **82**, 2975 (1985); **82**, 2994 (1985).
61. S. Mukamel, K. Shan, and Y. J. Yan, in *Polycyclic Aromatic Hydrocarbons and Astrophysics*, (A. Leger and L. d'Hendercourt, and N. Boccara, NATO ASI Series, Vol. C **191**, pp. 129). Reidel, Dordrecht, (1986); K. Shan, Y. J. Yan, and S. Mukamel *J. Chem. Phys.* **87**, 2021 (1987).
62. W. H. Louisell, *Quantum Statistical Properties of Radiation*. Wiley, New York, 1973.
63. S. Mukamel and E. Hanamura, *Phys. Rev. A* **33**, 1099 (1986); E. Hanamura and S. Mukamel, *J. Opt. Soc. Am. B* **3**, 1124 (1986).
64. Y. J. Yan and S. Mukamel *J. Chem. Phys.* **86**, 6085 (1987).
65. R. A. Marcus, *J. Chem. Phys.* **24**, 979 (1956).
66. Yu. T. Mazurenko and V. S. Udaltsov, *Opt. Spec.* **44**, 417 (1977); L. A. Hallidy and M. R. Topp, *J. Phys. Chem.* **82**, 2415 (1978); E. W. Castner, M. Maroncelli, and G. R. Fleming, *J. Chem. Phys.* **86**, 1090 (1987); M. Maroncelli, E. W. Castner, S. P. Webb, and G. R. Fleming, in *Ultrafast Phenomena V* (G. R. Fleming and A. E. Siegman, eds.). Springer-Verlag, Berlin, 1986.
67. Yu. T. Mazurenko and N. G. Bakshiev, *Opt. Spec.* **28**, 490 (1970); B. Bagchi, D. W. Oxtoby, and G. R. Fleming, *Chem. Phys.* **86**, 257 (1984); G. Van der Zwan and J. T. Hynes, *J. Phys. Chem.* **89**, 4181 (1985).
68. R. F. Loring, Y. J. Yan, and S. Mukamel, *Chem. Phys. Lett.* **135**, 23 (1987); *J. Phys. Chem.* **91**, 1302 (1987); *J. Chem. Phys.* **87**, (1987) (in press).
69. D. L. Huber, *Phys. Rev.* **170**, 418 (1968); **178**, 93 (1969); **187**, 392 (1969); A. Omont, E. W. Smith, and J. Cooper, *Astrophys. J.* **175**, 185 (1972).
70. P. F. Liao, J. E. Bjorkholm, and P. R. Berman, *Phys. Rev. A* **20**, 1489 (1977); J. L. Carlsten, A. Szoke, and M. G. Raymer, *Phys. Rev. A* **15**, 1029 (1977).
71. R. M. Hochstrasser and C. A. Nyi, *J. Chem. Phys.* **70**, 1112 (1979); J. M. Friedman and R. M. Hochstrasser, *Chem. Phys. Lett.* **33**, 225 (1975); *Chem. Phys.* **6**, 155 (1974).
72. Y. R. Shen, *Phys. Rev. B* **9**, 622 (1974).
73. K. Burnett, *Phys. Rep.* **118**, 339 (1985).
74. Y. Toyozawa, *J. Phys. Soc. Jpn.* **41**, 400 (1976); A. Kotani and Y. Toyozawa, *J. Phys. Soc. Jpn.* **41**, 1699 (1976).
75. V. Hizhnyakov and I. Tehver, *Phys. Stat. Solidi* **21**, 755 (1967); *Opt. Comm.* **32**, 419 (1980).
76. H. A. Kramers and W. Heisenberg, *Z. Phys.* **31**, 681 (1925).

77. R. G. Breene, *Theories of Spectral Lineshapes* Wiley, New York, 1981.
78. D. Grimbert and S. Mukamel, *J. Chem. Phys.* **75**, 1958 (1981); **76**, 834 (1982).
79. S. Mukamel, *Phys. Rev. A* **26**, 617 (1982).
80. S. Mukamel and D. Grimbert, *Optics Comm.* **40**, 421 (1982).
81. J. J. Markham, *Rev. Mod. Phys.* **31**, 956 (1959).
82. R. Kubo and Y. Toyozawa, *Prog. Theo. Phys.* **13**, 160 (1955).
83. S. Mukamel, *J. Chem. Phys.* **77**, 173 (1982); A. Warshel, P. S. Stern, and S. Mukamel, *J. Chem. Phys.* **78**, 7498 (1983).
84. S. Mukamel, *J. Phys. Chem.* **88**, 3185 (1984).
85. J. Chesnoy and J. J. Weis, *J. Chem. Phys.* **84**, 5378 (1986); M. J. Saxton and J. M. Deutch, *J. Chem. Phys.* **60**, 2800 (1974).
86. D. Thirumalai, E. J. Bruskin, and B. J. Berne, *J. Chem. Phys.* **83**, 230 (1985).
87. L. Onsager, *J. Am. Chem. Soc.* **58**, 1486 (1936).
88. N. S. Baylis, *J. Chem. Phys.* **18**, 292 (1950).
89. C. J. F. Bottcher, *Theory of Electric Polarization.* Elsevier, Amsterdam, 1973, Vols. I, II.
90. J. Jortner and C. A. Coulson, *Mol. Phys.* **4**, 451 (1961); J. Jortner, *Mol. Phys.* **5**, 257 (1962).
91. D. Chandler, K. S. Schweizer, and P. G. Wolynes, *Phys. Rev. Lett.* **49**, 1100 (1982); K. S. Schweizer and D. Chandler, *J. Chem. Phys.* **78**, 4118 (1983).
92. R. W. Hall and P. G. Wolynes, *J. Chem. Phys.* **83**, 3214 (1985).
93. N. Bloembergen, E. M. Purcell, and R. V. Pound, *Phys. Rev.* **73**, 679 (1948).
94. P. W. Anderson and P. R. Weiss, *Rev. Mod. Phys.* **25**, 269 (1953).
95. R. Kubo, in *Fluctuations, Relaxation and Resonance in Magnetic Systems* (D. ter Haar, ed.). Plenum, New York, 1962, p. 23.
96. J. Sue and S. Mukamel (unpublished)
97. N. G. Van Kampen, *Stochastic Processes in Physics and Chemistry.* North-Holland, Amsterdam, 1981.
98. See papers in *Farad. Disc. Chem. Soc.* **75** (1983).
99. D. H. Levy, *Ann. Rev. Phys. Chem.* **31**, 197 (1980).
100. C. S. Parmenter, *J. Phys. Chem.* **86**, 1735 (1982); *Farad. Disc. Chem. Soc.* **75**, 7 (1983); D. A. Dolson, K. W. Holtzclaw, S. H. Lee, S. Munchak, C. S. Parmenter, and B. M. Stone, *Laser Chem.* **2**, 271 (1983); K. W. Holtzclaw and C. S. Parmenter, *J. Chem. Phys.* **84**, 1099 (1986); D. A. Dolson, K. W. Holtzclaw, D. B. Moss, and C. S. Parmenter, *J. Chem. Phys.* **84**, 1119 (1986).
101. J. B. Hopkins, D. E. Powers, S. Mukamel, and R. E. Smalley, *J. Chem. Phys.* **72**, 5049 (1980).
102. S. Mukamel, *J. Chem. Phys.* **82**, 2867 (1985).
103. G. Herzberg, *Molecular Spectra and Molecular Structure.* Van Nostrand, New York, 1966.
104. R. Islampour and S. Mukamel, *J. Chem. Phys.* **80**, 5487 (1984); *Chem. Phys. Lett.* **107**, 239 (1984).
105. S. Mukamel and K. Shan, *J. Phys. Chem.* **89**, 2447 (1985); *Chem. Phys. Lett.* **117**, 489 (1985).
106. J. Sue and S. Mukamel, *Chem. Phys. Lett.* **107**, 398 (1984).
107. J. Grad, Y. J. Yan, and S. Mukamel, *Chem. Phys. Lett.* **134**, 291 (1987); J. Grad, Y. J. Yan, A. Haque, and S. Mukamel, *J. Chem. Phys.* **86**, 3441 (1987).